Controls on Voisey Bay –type magmatic Cu-Ni mineralisation: A case history from the Caroline and Harcus Giles Complex intrusions, SA

Thesis submitted in accordance with the requirements of the University of Adelaide for an Honours Degree in Geology

Callum John Richardson

November 2013

THE UNIVERSITY of ADELAIDE

MAGMATIC CU-NI MINERALISATION: GILES COMPLEX

ABSTRACT

Intrusion related magmatic copper-nickel sulphide ore bodies are of great economic interest but there are a variety of different factors that play a role in their development in the crust. The evolution of magma through the crust has a great impact on the potential for an economic ore body to be formed and as such different intrusions are the subject of study to better understand their evolution in this regard. This study investigates two intrusions, Caroline and Harcus, that are part of the larger *Giles Complex Intrusions*, found in the Musgrave province in far north of South Australia.

Analysis of petrography, mineral chemistry and whole rock chemistry was undertaken including Nd-Sr isotopic analysis. From this it was possible to define that the Caroline intrusion has experienced ~35% crustal assimilation in its evolution and has not experienced a sulphide saturation event before emplacement. The Harcus intrusion has experienced ~15% crustal assimilation in its evolution and has likely already experience a sulphide saturation event in its evolution. It was also possible to define that the Harcus intrusion appeared to be a trapped melt and not a layered intrusion like that of the Caroline intrusion. From the work that was undertaken a model composition for the initial melt from which both intrusions formed was defined. This was tested using crystallisation modelling and was found to be an adequate match to the different compositions of the intrusions. An emplacement model for the two different intrusions has been proposed.

The more ideal economic target has been defined to be that of the Caroline intrusion as it has not experienced a prior episode of sulphide saturation.

KEYWORDS

Controls, Voisey Bay, Magmatic, Nickel, Copper, Sulphides, Musgraves, Caroline, Harcus, Giles Complex, WLIP

TABLE OF CONTENTS

LIST OF FIGURES

LIST OF TABLES

INTRODUCTION

One class of nickel-copper (Ni-Cu) mineralisation occurs within large layered mafic intrusions (Naldrett 1999, Lightfoot 2007, Maier & Groves 2011). It can be difficult to determine the exact location of such economic nickel and copper deposits within these intrusions due to a variety of different factors that can influence the parental magma and as a result impact on the development of an ore body (Maier *et al.* 2001, Lightfoot 2007). These factors include those that dictate sulphur saturation, metal enrichment and sulphide localisation (Jugo 2010, Fiorentini *et al.* 2012, Ripley & Li 2013). The late Mesoproterozoic Giles complex (Wingate *et al.* 2004), hosted within the early Mesoproterozoic Musgrave Province in central Australia (Cawood & Korsch 2008, Wade *et al.* 2008), is a series of layered mafic-ultra mafic intrusions (Wingate *et al.* 2004) that are the focus of a series of ongoing exploration programs for magmatic Ni-Cu sulphide accumulations (Woodhouse & Gum 2005, Rutherford 2011). One economic Ni-Cu deposit has been located within the Nebo-Babel intrusion in Western Australia (Baker & Waugh 2005, Godel *et al.* 2011, Seat *et al.* 2011). In this paper I intend to define a geochemical model for the evolution of the parental magma for two of the Giles intrusions (Caroline and Harcus) and to discuss their sulphide mineralisation potential. This paper will argue that the geochemical evidence shows there is potential for another economic Ni-Cu deposit to be located within the South Australia section of the Musgrave Province associated with one of the Giles complex layered mafic intrusions.

GEOLOGICAL SETTING

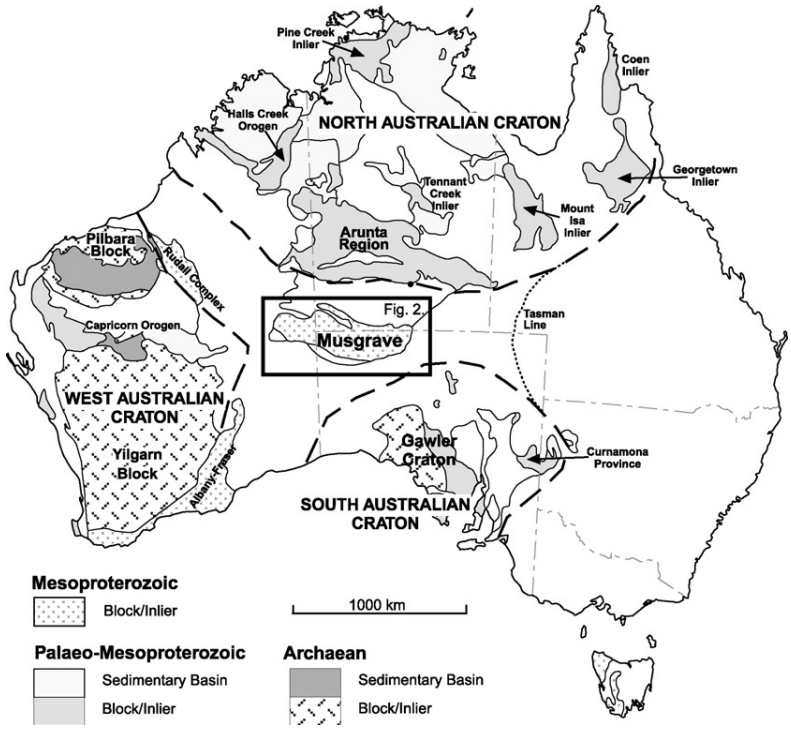

Figure 1 - Map of Australia displaying the locations of Archaean cratons and Palaeo-Mesoproterozoic terrains. Inset: Rectangle designates location of Musgrave Province. Figure adapted from Wade *et al.* (2008).

The Central Australian Musgrave province, figure 1 and 3 exposes exhumed Mesoproterozoic basement adjacent to mid Neoproterozoic to Phanerozoic basins (Wade *et al.* 2008). The Musgrave province is bound to the north by the mid-Neoproterozoic to mid Palaeozoic Amadeus basin, to the south and west by the mid-Neoproterozoic to early Palaeozoic Officer Basin, and to the east by the Permian to Mesozoic Eromanga basin. The Musgrave province is bisected by the late-Neoproterozoic, south dipping Woodroffe Thrust (Aitken & Betts 2008, Cawood & Korsch 2008, Wade *et al.* 2008, Aitken & Betts 2009b). This thrust divides the Musgrave province into two sub domains; the amphibolite facies Mulga Park sub domain to the north and the southerly Fregon sub domain ranging from granulite to upper amphibolite (Aitken & Betts 2009a). This area is the meeting point between three

of Australia's cratons with the Gawler Craton to the south, the North Australian to the north and the Western Australian craton to the west; the Yilgarn and Pilbara cratons (Cawood & Korsch 2008).

The Musgrave province comprises a series of different intrusion events that are part of the Wakaruna Large Igneous Provence (WLIP) (Wingate *et al.* 2004, Pirajno & Hoatson 2012). This can be seen below in figure 2. The Musgrave province intrusions are referred to as the Giles Intrusions or the *Giles event*. The WLIP including the Giles intrusions are amongst the most voluminous Large Igneous province (LIP) in the world (Evins *et al.* 2010). They are thought to be associated with either the upwelling of a large intraplate mantle plume (Evins *et al.* 2010) or from the melting of Sub continental Lithospheric mantle (Wade *et al.* 2008) due to an undefined thermal disturbance.

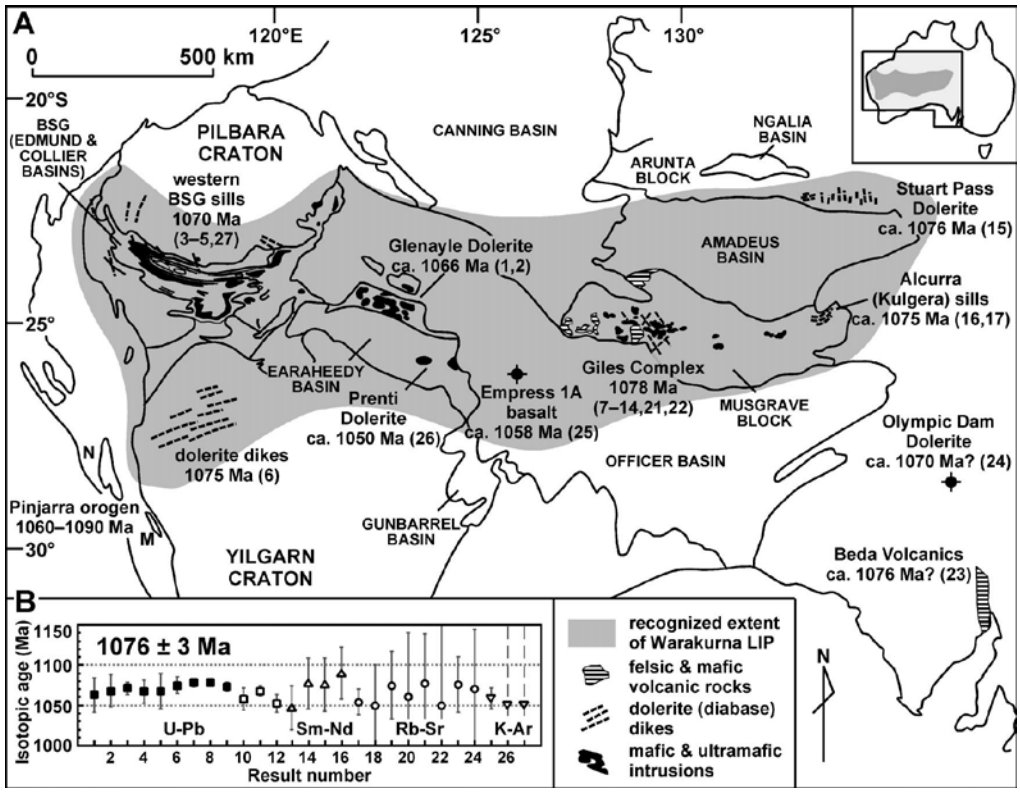

Figure 2 – (a): Simplified geology of southwest Australia, showing distribution of ca. 1075 Ma igneous rocks of Warakurna large igneous province (LIP). Numbers after rock ages refer to plot (b). BSG— Bangemall Supergroup; N—Northampton inlier; M—Mullingarra inlier. B:Isotopic age

determinations for rocks of Warakurna LIP, grouped according to isotopic system. Figure adapted from Wingate *et al.* (2004).

This Musgrave province is composed of varied lithological units that range in age from earliest Mesoproterozoic to Neoproterozoic. The lithologies of the Musgrave Province are varied and collectively referred to as the Musgravian Gneiss (Cawood & Korsch 2008). Within the Fregon sub domain the Musgravian Gneiss is termed the Birksgate Complex and in the Mulga Park sub domain it is termed the Olia Gneiss. This gneiss is mainly felsic in composition in both of the domains with a minor mafic layering present also (Wade *et al.* 2008).

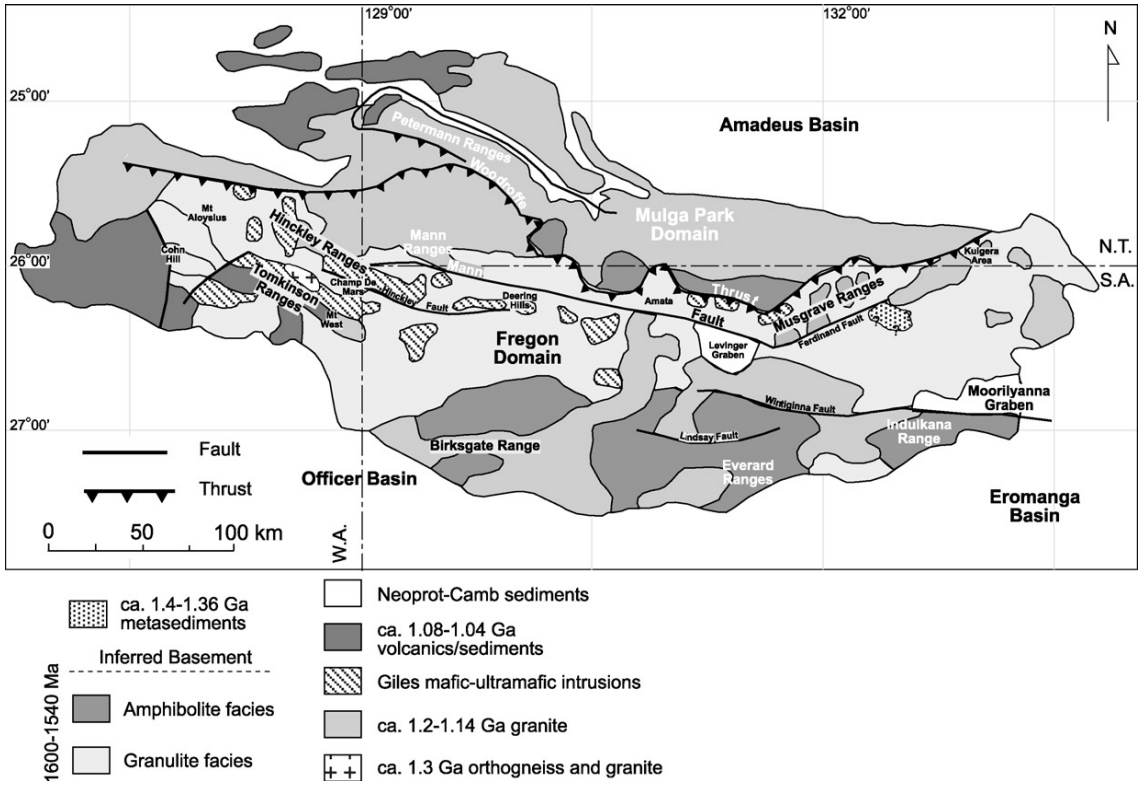

Figure 3 - Simplified geological map of the Musgrave Province showing locations of areas discussed in text. Figure adapted from Wade *et al.* (2008).

MAFIC INTRUSION HOSTED NI-CU-PGE MINERALISATION SYSTEMS.

An important class of magmatic nickel – copper ore systems (+/-PGEs) are hosted by layered mafic intrusive complexes. Classic examples of this ore deposit group include;

Voisey's Bay, Jinchuan and to a certain degree Sudbury (Naldrett 1997, 1999, Naldrett 2004). The genesis of these sulphide systems is closely related to the magmatic petrogenesis of their host mafic intrusions. These sulphide ores are hosted by highly magnesian, mantle derived (tholeiitic – picritic), ultramafic to mafic igneous suites (Maier & Groves 2011). Prior studies suggest that these parental magmas may be plume or rift-related (Maier *et al.* 2001, Naldrett 2004, Maier & Groves 2011).

During the evolution of the magma, the silicate melt may become saturated in sulphur to form a separate sulphide liquid (Ripley & Li 2013). Cu, Ni and PGE elements are then partitioned to this sulphide liquid due to the higher partition coefficient of these elements into the sulphide phase. The initially formed sulphide melt that develops as an immiscible phase at magmatic temperatures has a composition that eventually unmixes during crystallisation and cooling to form a number of sulphide species. The composition of the initial sulphide phase has been the subject of studies in the past (Guo *et al.* 1999, Fleet 2006, Lorand & Grégoire 2006) and is a monosulphide solid solution (MSS) and it is from this sulphide that the different sulphides species form when more appropriate thermodynamic conditions are reached (Guo *et al.* 1999, Fleet 2006). Due to the physical manner in which the sulphide liquid separates from the silicate melt, (often from the silicate melt at the same time as silicate phases are precipitating and accumulating) magmatic Ni-Cu sulphide bodies are typically small and irregular, forming in lava channels, dykes, sills, and chonoliths (Maier & Groves 2011). These are all interpreted to be the magma feeder channels to overlying or distal and increasingly evolved magmatic system. Collection of sulphide liquids may occur where the magma is able to slow in its ascent and pond in zones of reduced flow leading to density-controlled settling (Maier *et al.* 2001, Li *et al.* 2003).

The host mineralogies for Ni-Cu systems vary between the different intrusive systems due to the varying rock types and emplacement conditions. Host rock types are typically cumulate ultra mafic to mafic rocks and include dunite (Jinchuan), harzburgite (Kabanga), pyroxenite (Santa Rita, Selebi Phikwe), olivine gabbro (Noril'sk), gabbronorite (Sudbury) and troctolite (Voisey's Bay) (Naldrett 1997, 1999, Maier *et al.* 2001, Maier & Groves 2011). In these suites particularly the mafic-ultra mafic rocks are of a cumulative origin. The main economic mineralogies for Ni-Cu systems remain typically the same across the different host mineralogies with the assemblage including pyrite, pyrrhotite, pentlandite, and chalcopyrite (Maier & Groves 2011). Millerite also occurs in some suites.

This work focuses on intrusive bodies of the SA Giles complex. These are correlatives of the Nebo-Babel intrusions and deposit in Western Australia (Baker & Waugh 2005, Seat *et al.* 2007, Seat *et al.* 2009, Evins *et al.* 2010, Godel *et al.* 2011, Seat *et al.* 2011) (discussed more specifically later in this section). These suites are composed of a single or two pyroxene cumulates (pyroxenites) with or without plagioclase and also as gabbros and gabbro norite (Seat *et al.* 2007). The sulphides could potentially form large ore bodies occur as texturally intercumulus grains (Godel *et al.* 2011). Concentration of these sulphides results from collection in basal areas due to density and gravitational forces (Maier & Groves 2011). This process may have resulted in the larger lenses of massive sulphide that for the economic target within the Nebo-Babel deposit (Godel *et al.* 2011). In the Woodroofe and Harcas systems studied here we have good evidence that immiscible, dense sulphide liquid has accumulated together with orthopyroxene to formed sulphide-enriched orthopyroxenite cumulates.

Because these deposits are associated with a variety of magma systems and because their feeder conduits they can be difficult to locate the quest for the discovery of these types of deposits continues. Advances are being made to improve the models that are used for exploration (Lightfoot 2007) coupled with the improving geophysical techniques that can be made available (King 2007) and this can only act to increase the probability that we will be able to locate the deposits that different models suggest should be out there (Mamuse *et al.* 2010).

SULPHIDE SATURATION

A key issue in these systems is to understand which factors control the onset of sulphide saturation in evolving mafic layered intrusions Factors that can play a role in the sulphur evolution of magma as it rises include; the degree of partial melting of the source mantle, the oxygen fugacity of the magma (Jugo 2010), and the impact of assimilation of reducing materials and sulphur during emplacement (Lightfoot 2007, Seat *et al.* 2009, Jugo 2010, Maier & Groves 2011, Ripley & Li 2013) and the impact of the amount of FeO in the melt (Jugo 2010).

Jugo (2010) has shown that the degree of partial melting of the source mantle is a controlling factor on the amount of sulphur in the resultant melt. This author states that the degree of partial melting must be at least in the order of 25% or greater in order to eliminate refractory sulphide phases from the unmelted mantle residue. He also suggests that the sulphur solubility in the mafic magma is very dependent on the oxidation state of sulphur. Reduced S as S^{2-},is much less soluble than the mode oxidised S^{6+} species. The proportions of the two sulphur species are a function of oxygen fugacity (fO_2) and when fO_2 increases the ratio increases and causes the sulphur solubility at sulphur saturation (SCSS) to increase exponentially. This means that more oxidised

differentiating mafic magmas may evolve to increasing S content and remain undepleted in Cu, Ni and PGEs. Reduction of this system may then cause catastrophic sulphide saturation and a sudden decline in the Cu, Ni and PGE content of the silicate melt. Work to better understand the different concentrations of sulphur when sulphur saturation is achieved has been undertaken by Liu *et al.* (2007).

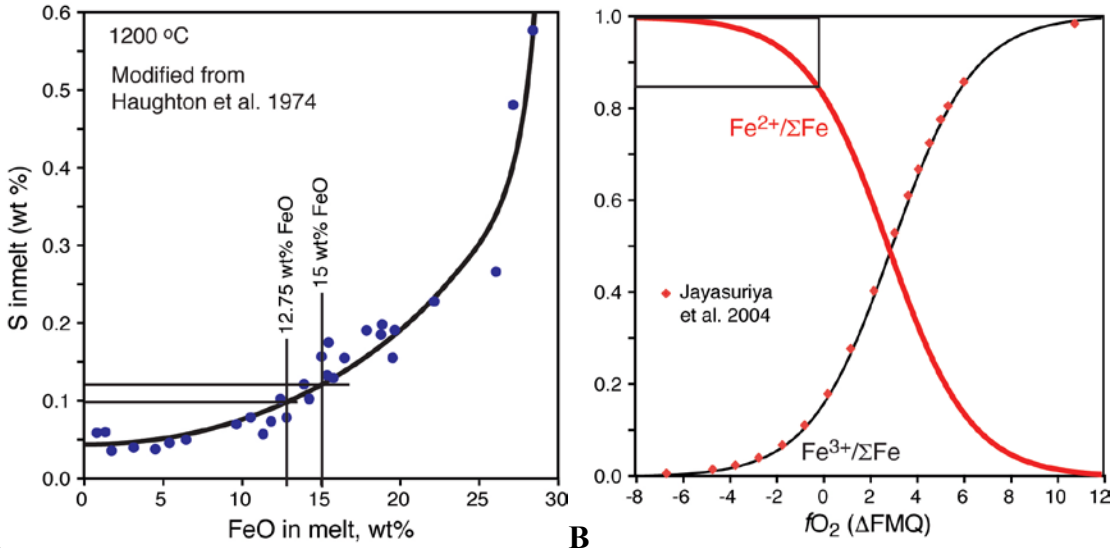

Figure 4 - (a) Sulfur content at sulfide saturation as a function of FeO (modified from Haughton et al. 1974) showing the effect of decreasing FeO from 15 wt% FeO to 12.75 wt% on SCSS.

(b) Change in the relative proportions of Fe3+ (black curve) and Fe2+ (red curve) with increasing *f*O2 (based on the data of Jayasuriya *et al.* (2004)) (figures adapted from Jugo (2010))

The assimilation and cannibalisation of wall rocks into which the ore bodies intrude can have a large impact on the sulphur saturation of the system which in turn has an impact on the ability of the system to generate an economic ore body. The different interactions that can take place between a magma and the wall rocks that may lead to sulphide saturation include; the assimilation of sulphide bearing rocks (Naldrett 1999, Maier & Groves 2011), the assimilation of reducing lithologies, such as coal measures or graphite rich beds, causing a decrease in the redox state of the system (Jugo 2010) and the assimilation of siliceous, but sulphur poor rocks which can also lead to the reduction in sulphur solubility (Seat *et al.* 2009, Maier & Groves 2011, Ripley & Li 2013).

NEBO BABEL

The Nebo-Babel deposit is an example of an economic Ni-Cu deposit that has been located within the Musgrave Province. This deposit was discovered in 2000 after an exploration program undertaken by WMC (Baker & Waugh 2005) and is located within the West Australian area of the Musgrave province (Seat *et al.* 2007). This deposit is a hosted by a complex chonolithic (tube-like), zoned, gabbronorite intrusion that is part of the Giles complex within the WLIP. The deposit at Nebo-Babel has some unique characteristics when compared to other intrusive Ni-Cu deposits around the world because it shows evidence of sulphur saturation without significant levels of crustal sulphur assimilation (Seat *et al.* 2009), this gives support to the notion that sulphur rich country rocks are not always critical in the formation of magmatic Ni-Cu deposits as suggested by Fiorentini *et al.* (2012).

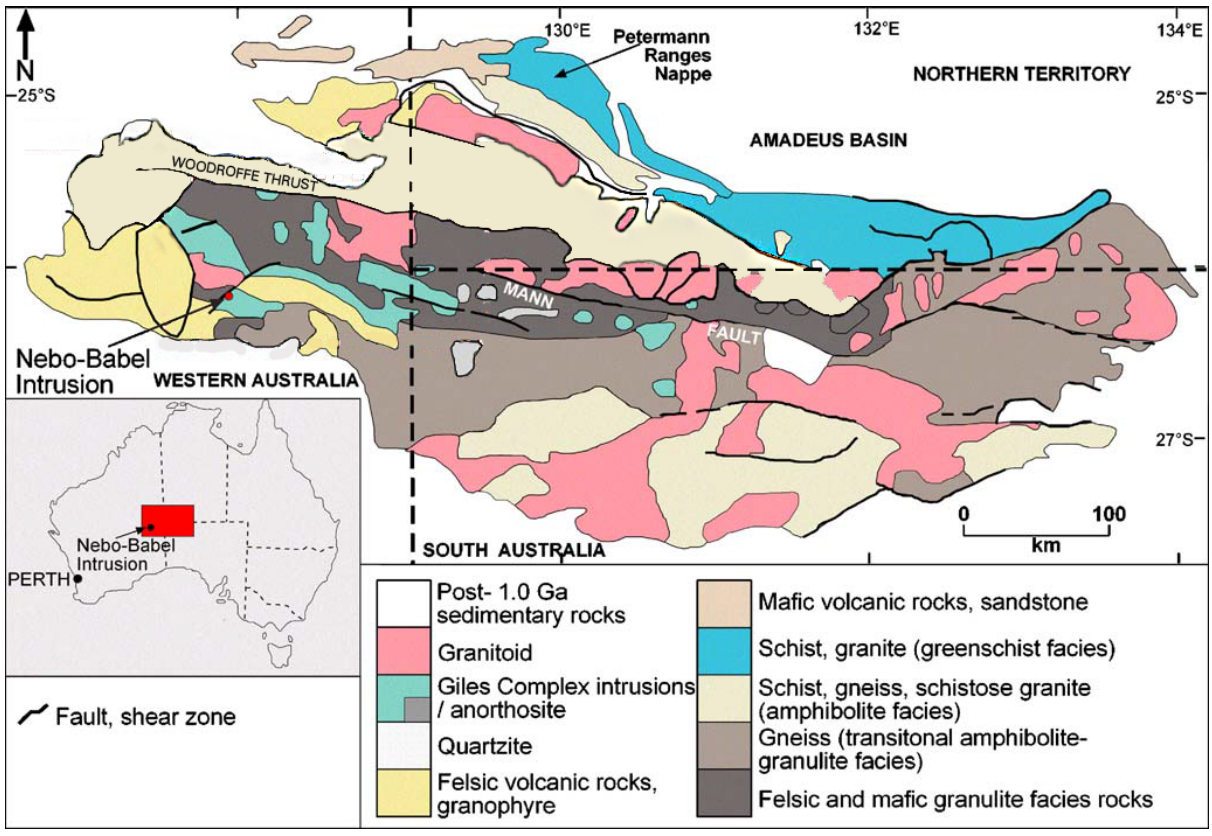

Figure 5 - Regional geology of the Musgrave Block with Nebo Babel Highlighted. Map Adapted from Seat *et al.* (2007)

The Nebo-Babel ore bodies are probably analogous to those anticipated in the Caroline and Harcus intrusions. This paper will work with data and samples from drill core taken from exploration licenses in the vicinity of Mt Harcus, Mt Woodroffe and Mt Caroline in the far north of South Australia. This project intends to build up a picture of the magmatic evolution of some of the Giles intrusions and to examine the variables that can impact on the formation of economic ore bodies in these bodies.

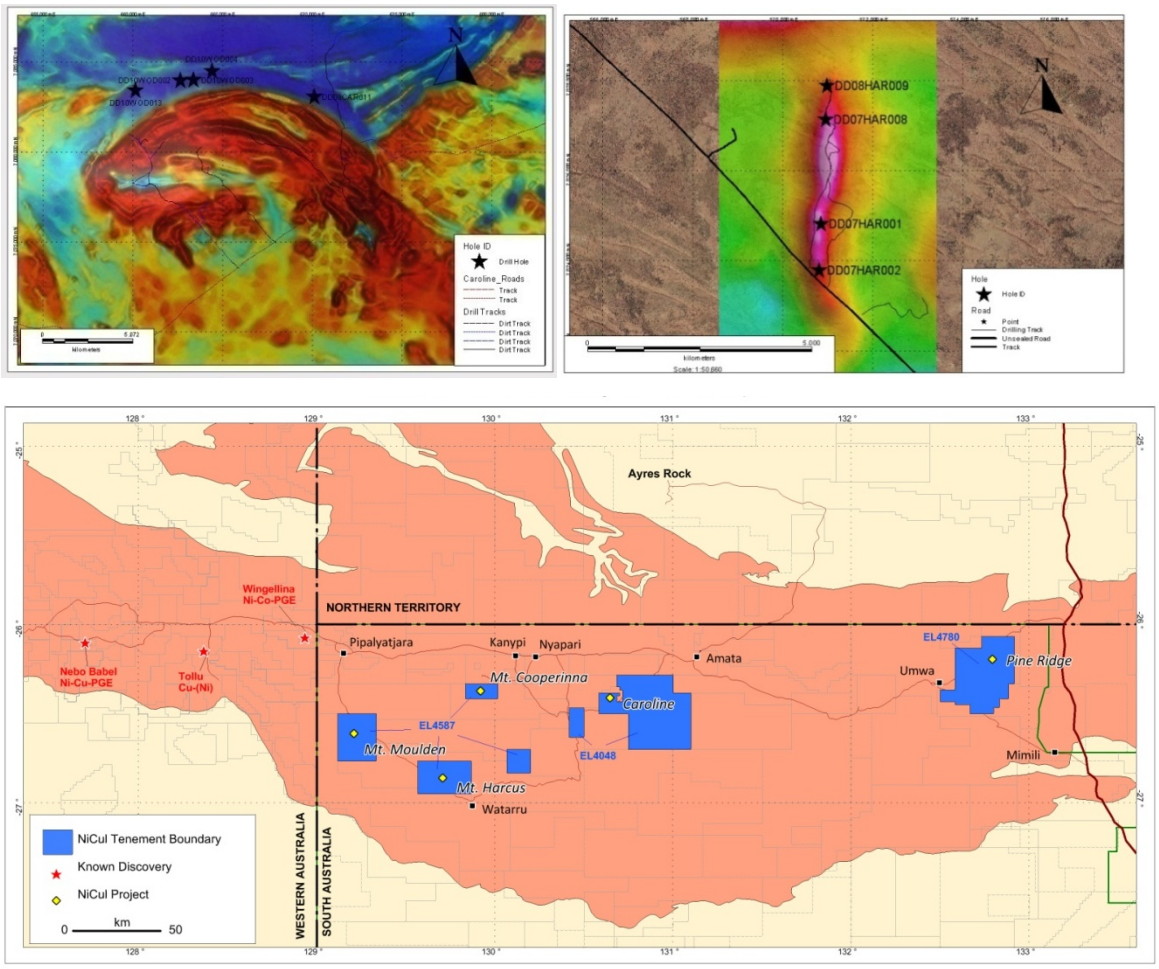

Figure 6 - clockwise from top left, reduced to poles map of magnetic intensity of the Caroline intrusion with drill holes identified. Complete Bouguer anomaly map of the Harcus intrusion with drill holes identified. Map of the different exploration tenements with other Ni-Cu projects identified. Figure adapted from Todd (2013)

METHODS

Sampling and sample preparation

Sampling was undertaken after scrutiny of geochemical data (Rutherford & Clifford 2008, Rutherford 2010, 2011) to locate targets of interest with a focus on concentration of nickel, copper, iron and magnesium number. These samples were collected from HQ or NQ half or quarter core samples located at the PNN core storage facility in Smithfield, South Australia. These samples were then prepared for use in the sectioning and lapidary areas of the Mawson Laboratories, School of Earth and Environmental Sciences, University of Adelaide.

Petrography

Optical petrography was undertaken on 39 polished thin section slides that were prepared at Adelaide Petrographic Laboratories PTY LTD located in Norwood, SA. Analysis of each sample was undertaken including major mineralogical composition and investigation of any sulphide/oxide phases present. This was undertaken at the Mawson Laboratories, School of Earth and Environmental Sciences, University of Adelaide.

Mineral Geochemistry

Mineral geochemistry was undertaken on thirty prepared polished thin sections with analyses undertaken on pyroxenes, plagioclase and sulphides. This was conducted on the CAMECA SXFive Electron Microprobe located at Adelaide Microscopy, Adelaide. The elements were determined using an acceleration voltage of 20 kV, a beam current of 20nA for the silicate minerals and an acceleration voltage of 20 kV, a beam current

of 15nA for the sulphide minerals. Counting times for major and trace elements varied relative to the elements and can be found in the appropriate appendix. Under such conditions, the detection limit is 0.015w/w% for trace elements.

Whole rock Geochemistry

Twenty samples were prepared and analysed for minor and trace elements and loss on ignition (LOI) at the Mawson Laboratories, School of Earth and Environmental Sciences, University of Adelaide. The element concentrations were determined by using a combination of X-ray fluorescence spectroscopy using a Philips PW 1480 X-ray Fluorescence Spectrometer and solution based inductively coupled plasma-mass spectrometry (ICP-MS) analysis at Adelaide Microscopy, Adelaide. Accuracy and precision were tested by use of international standards and repeat measurements. Accuracy and precision of this dataset was determined to be within 3% for all included elements.

Sm-Nd-Sr Isotopes

Whole-rock Sm-Nd-Sr isotope analyses were carried out on six samples at the Mawson Laboratories, School of Earth and Environmental Sciences, University of Adelaide (Australia), using a Finnigan MAT262 thermal ionization mass spectrometer (TIMS). A detailed methodology can be found in the appropriate appendix.

OBSERVATIONS AND RESULTS

Petrography and mineral chemistry

A summary table of the results from the petrography can be found in table 1, and 2.

Table 1 - Petrographic analysis of the Caroline and Harcus intrusion including core description

Intrusion	Drill hole	Depth	Core lithology	Modal mineralogy	Sulphide species present	Stratigraphic description 1
Caroline	DD10WOD002	45	Grey cumulate gabbronorite	Plag: 40 Px: 60	rare	This hole contains five stratigraphically groupable areas as defined by their visible textures within the core. These include a cumulate band from 7.9m to 109.4m in depth. At this point there is a transition with a banded megacrystic zone and then the second zone of banded gabbronorite and leucogabbronorite with some minor chlorite shears from 135m to approximatelty 210m, the bottom of this zone is brecciated by a later shearing event. The third zone is a layered, banded gabbronorite of a different colour from approimately 210m to 227m where it then enters into a zone of interlayered lithologies of layered and megacrystic gabbronorite and pyroxenites. Subsequent to this it then enters a zone of banded, layered gabbronorite from 240m through to 266m. From 266m through to the termination of the hole at 288m it is a banded leucogabbronorite.
		67	pink-grey cumulate gabbronorite	Plag: 45 Px: 50	5%	
		110	pink-grey banded megacrystic gabbronorite	Plag: 75 Opx: 5 Cpx: 20		
		130	green sheared leucogabbronorite	Plag: 10 Opx: 30 Cpx: 50	10% - pyrrhotite, minor chalcopyrite	
		135	grey banded gabbronorite	Plag: 20 Opx: 40 Cpx: 30	10% - pyrrhotite, minor chalcopyrite	
		150	grey banded gabbronorite	Plag: 15 Cpx: 80	5% - Pyrrhotite, minor Chalcopyrite	
		153	grey banded gabbronorite	Plag: 10 Px: 90	rare	
	DD10WOD003	65	pink-grey weakly banded gabbronorite	Plag: 50 Opx: 20 Cpx: 30	rare	This hole contains two zones of groupable lithologies that then contain their own complexities. The first zone is from 11m through to 60m and is a grey to a pink-grey layered gabbronorite with some zones of leucogabbronorite. The second group of lithologies is from 60m until the end of hole at 247.5m. Within this second group there appears to be a cyclic system of layered/banded gabbronorites grading down into a megacrystic zone which then cycles again, the thinknesses of these cycles vary from single meters through to 50 meter zones.
		75	pink-grey weakly banded gabbronorite	Plag: 50 Opx: 30 Cpx: 20		
		85	pink-grey weakly layered leucogabbronorite	Plag: 50 Px: 40	10% - pyrrhotite, minor chalcopyrite	
	DD10WOD004	190	grey cumulate pyroxenite	Plag: 40 Opx: 20 Cpx: 30	10% - pyrrhotite, minor chalcopyrite	This drill hole contains three groupable lithologies. The first of these is a large series of cyclic bands of layered gabbronorite that then grades down into megacrystic gabbronorite. These cycles appear to be over the course of 5 meters with the largest cycle being 15 meters. these cycles extend from 3.2m through to a depth of 187m. The second lithology is that of a cumulate pyroxenite-gabbronorite that extends from 187m through to 226m where it terminates at a megacrystic zone. The third lithology is that of a pink and grey cumulate gabbronorite-pyroxenite at extends from 226m through to the end of hole at 252m.
		215	grey brecciated pyroxenite	Plag: 10 Px: 80	10%	
		220	Grey cumulate gabbronorite	Plag: 20 Opx: 40 Cpx: 30	10%	

Table 2 - petrography results continued

Intrusion	Drill hole	depth	Core lithology	Modal mineralogy	Sulphide species present	Stratigraphic description 1
Caroline	DD10WOD013	100	mineralised megacrystic gabbronorite	Plag: 30 Opx: 20 Cpx: 45	5%	This drill hole contains four groupable lithologies. The first of these was from 3.8m to 41m and was a grey gabbronorite with primary igneous textures but not banding or cumulate textures. The second layer was a variably igneous texture to megacrystic grey gabbronorite and was from 41m through to 83.5m. The third lithology was that of a megacrystic gabbronorite that extended from 83.5m to 157m. The fourth lithology was that of a broadly banded variably mineralised gabbronorite that extended from 157m till the end of hole at 251m.
		104	grey banded gabbronorite	Plag: 60 Opx: 15 Cpx: 20	5%	
		125	grey megacrystic gabbronorite	Plag: 50 Opx: 25 Cpx: 25		
	DD09CAR011	230	grey foliated leuco gabbroic gneiss	Plag: 40 Opx: 30 Cpx: 30	rare	This drill hole contains two groupable lithologies. The first of these being from 4m through to 67m which is a layered white-grey gabbro which terminates in a troctolitic, megacrystic layer. The second lithology is from 67m through to the end of hole at 452m and is a foliated leucogabbroic gneiss-gabbroic gneiss. Within this second lithology there is no apparent cycling although there are occasional layers that contain unfoliated grains and different visual colours.
		240	grey foliated leuco gabbroic gneiss	Plag: 60 Opx: 10 Cpx: 30	rare	
		305	grey foliated gabbroic gneiss	Plag:20 Opx: 30 Cpx 50	rare	
		310	pink foliated leuco gabbroic gneiss	Plag: 70 Opx: 10 Cpx: 20	rare	
Harcus	DD07HAR001	80	grey-igneous gabbro	Plag: 40 Qtz: 10 Cpx:20 Opx: 20	10% - pyrrhotite, minor chalcopyrite	Two main lithologies within this core are related to the Giles Complex intrusions. The first of these is from 5.8m through to 171m and is composed of a variably banded gabbro. The second of these lithologies extends from 171m through to the contact zone between the intrusion and the country rock at approxiamately 209m. Late dykes associated with the Amata suite do cross cut both litholgies at different points.
		90	grey-igneous gabbro	Plag: 45 Cpx: 50 late Qtz:5	minor - Pyrrhotite, chalcopyrite	
		150	grey-igneous gabbro	Plag: 40 Cpx: 40 Opx: 10	10% - pyrrhotite	
		170	grey-igneous gabbro	Plag: 60 Px: 40	trace - Pyrrhotite	
	DD07HAR002	75	light grey finely speckled gabbro	Plag: 55 Px: 40	5% - Pyrrhotite	The lithologies of this core associated wih the Harcus intrusion are cryptic in nature and do not show obvious variation between the different zones of the core. Different areas do exist where the abundances of different sulphides and magnetite do vary. Details of this can be found in the technical report associated with this drilling period, listed in references.
		150	light grey finely speckled gabbro	Plag: 40 Px: 50	10% - Pyrrhotite	
		225	grey granophyric gabbro	Plag: 45 Cpx: 20 Opx: 20 Hbl: 10 (alteration)	5% - Pyrrhotite	
		324	grey fine grainular gabbro	Plag: 60 Px: 30	10% - Pyrrhotite	

Intrusion	Drill hole	Depth	Core lithology	Modal mineralogy	Sulphide species present	Stratigraphic description 1
Harcus	DD07HAR008	46	grey medium to coarse grained leucogabbro	Plag: 40 Px: 40 Chl	15% - Pyrrhotite, very minor Chalcopyrite	the lithologies of this core associated with the Harcus intrusion are cryptic in nature and show very little variation in appearances. This core however does show the greatest variation in magnesium number as calculated through core composites, within these different magnesium numbers there are specific plateaus that exist over large areas (Mg# 19 from 25m-100m, Mg# ~25 from 120m - 275m, Mg# 55 from 325m - 350m) which does suggest that they may be related to different lithologies.
		150	grey speckled coarse grained leucogabbro	Plag: 40 Px: 50	10% - Pyrrhotite	
		225	grey to yellowish aphanitic sulphidic gabbro	Plag: 40 Px: 40	20% - Pyrrhotite (70%), Chalcopyrite (30%)	
		300	grey medium grained gabbro	Plag: 45 Px: 50	5% - Pyrrhotite, minor Chalcopyrite	
		338	light grey to grey fine grained gabbro	Plag: 60 Px: 35	5% - Pyrrhotite, minor Chalcopyrite	
		370	grey fine to medium grained gabbro	Plag: 50 Px: 50	trace - Pyrrhotite	
	DD07HAR009	101	grey medium grained gabbro	Plag: 50 Px 35	5% - Pyrrhotite	The lithologies within this core associated with the Harcus intrusion are cryptic in nature and as such show little variation between the different layers and zones within the core. Differences can be seen when considering the abundances of the sulphides and oxides within the core. Overall the lithologies of the core are a variably textured grey to greenish grey gabbro.
		150	grey medium to coarse grained gabbro	Plag: 50 Px: 40	10% - Pyrrhotite	
		160	grey medium to coarse grained gabbro in association with the Amata dykes	Plag: 40 Px: 40	20% - Pyrrhotite (70%), Chalcopyrite (30%)	
		250	grey fine to medium grained gabbro	Plag: 60 Px: 25	15% - Pyrrhotite, very minor Chalcopyrite	
		260	grey fine to medium grained gabbro	Plag: 50 Px: 40	10% - Pyrrhotite	

CAROLINE

From the whole rock geochemical data (Rutherford & Clifford 2008, Rutherford 2010, 2011) four different diamond drill holes from the Woodroffe exploration license and one hole from the Caroline exploration licence were selected for sample collection, petrography and further analysis. Within these different diamond drill holes various different sections were selected and prepared due to chemical anomalies and areas of interest.

From the petrology that was undertaken it can be said that the majority of the Caroline intrusion is that of a gabbronorite in various different forms with locations of high concentrations of orthopyroxene bordering on pure orthopyroxenites. Within these different slides of interest the petrogenetic sequence can be said to have been orthopyroxene first, with associated interstitial MSS, clinopyroxenes were also present in smaller amounts in the samples. Subsequent to those phases the sequence was finished by the addition of later plagioclase. Spinels and occurrences of magnetite are also present within the core and are believed to have begun occurring at a similar time to that of plagioclase if not slightly before. Within the different samples there are different examples of exsolutions that can be seen within the pyroxenes with clinopyroxene interpreted to be exsolved from the orthopyroxene during petrogenesis. This suggests that the initial phases may have been formed with element concentrations that were, at later stages, less thermodynamically stable and as such they re-equilibrated to form the assemblages that we see in the various cores.

The sulphides phases that were present within the Caroline intrusion appear to have formed as part of an interstitial liquid as can be seen in the textures that they make with the well defined pyroxene grains around which they form, in addition to this, the lack of

inclusion of plagioclase in the sulphide species suggests that they formed at a stage before the plagioclase began to precipitate. The textures that they make and the spatial relationship of the different sulphides suggests that the sulphides formed as an initial MSS as suggested previously by the work of Fleet (2006) and then re-equilibrated to the sulphide species found within the core at a later stage. Detailed processes for the evolution of the different sulphide species through time can be found in the works of the afore mentioned author (Fleet 2006).

The sulphides that were present in the Caroline intrusion included pyrrhotite, chalcopyrite, millerite and pentlandite. The most dominant of these sulphides is that of pyrrhotite with chalcopyrite and pentlandite being less common. Millerite was only able to be located in isolated blebby intercumulate occurrences. Some chemical anomalies that were found within the different sulphides that were analyses were those of nickel concentrations obtained within some pyrrhotite grains that varied from below detection limits up to 7.5%w/w in multiple different drill holes and depths and a cobalt anomaly with concentrations in pyrrhotite grains up to 2.5%w/w in some isolated examples.

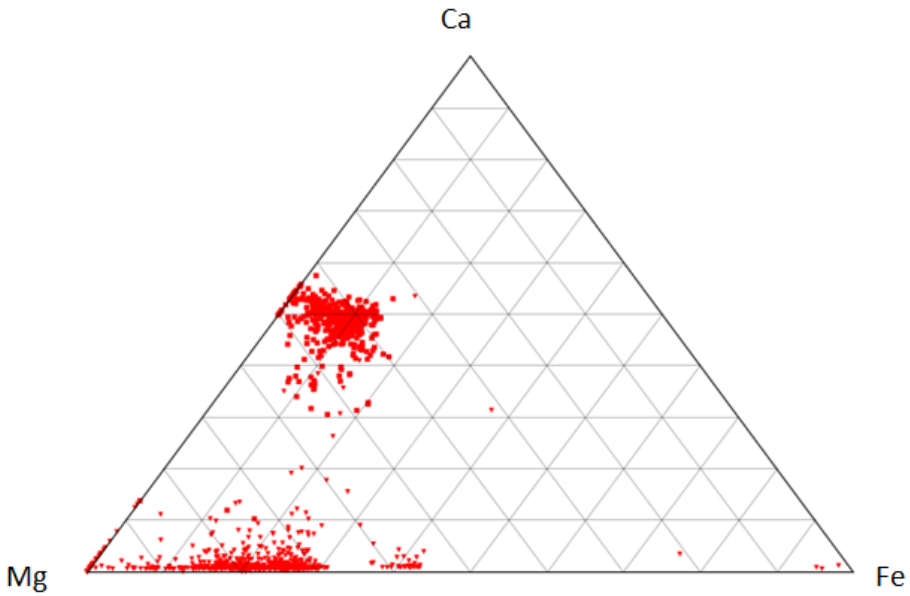

Figure 7 - a composite of pyroxene compositions throughout the various cores with colour pairs representing mineral compositions obtained from the same depth of core. squares = CPX triangles = OPX

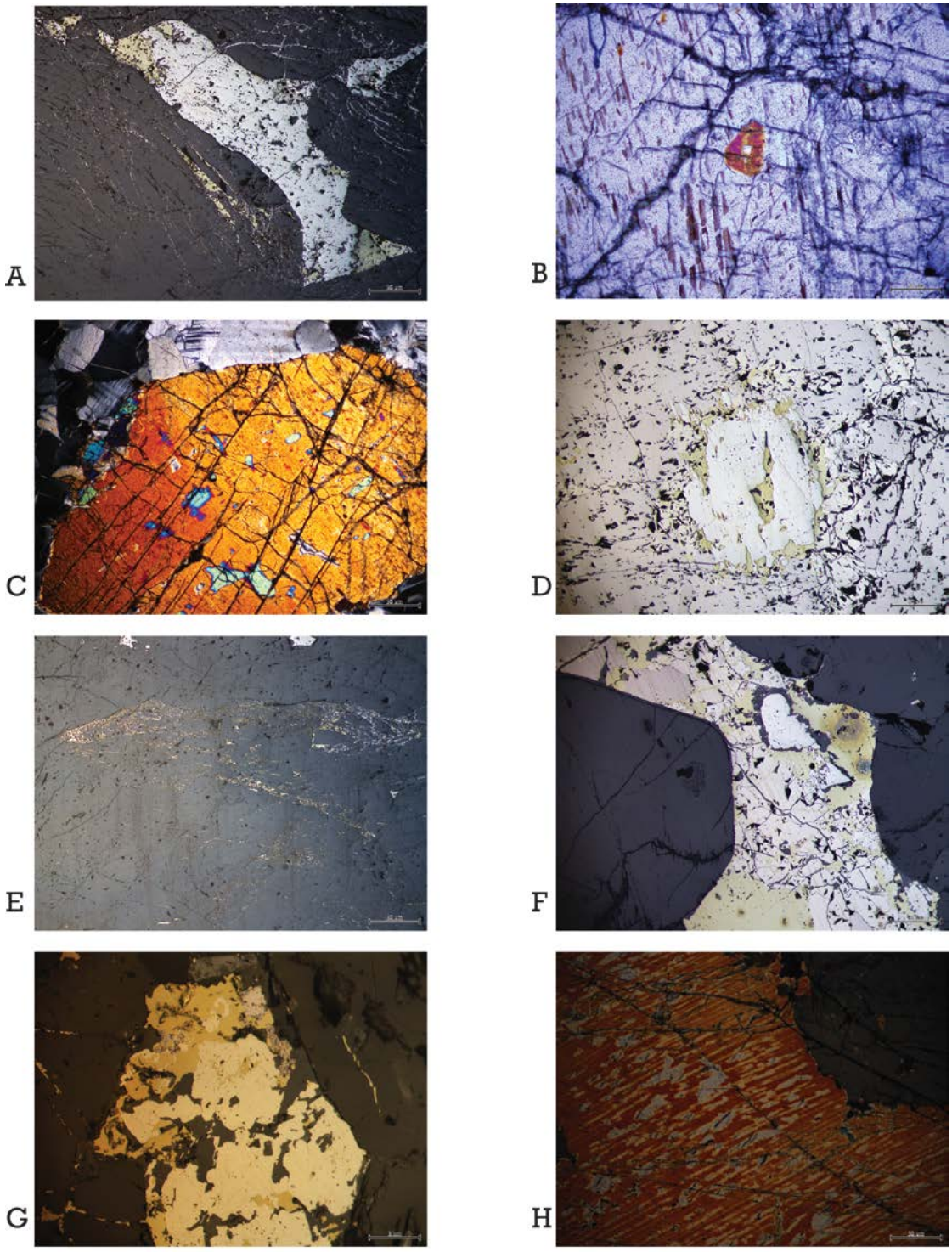

Figure 8 - Petrographic images of various slides from the Caroline intrusion. (A) Pyyrhotite and chalcopyrite in assemblage, from DD10WOD002 (B) A high birefringence inclusion within a pyroxene grain that also contains exsolutions, from DD10WOD003(C) Inclusions and exsolutions within a pyroxene grain, from DD10WOD003 (D) Pyrrhotite, chalcopyrite and very minor pentlandite able to be seen in assemblage, from DD10WOD004 (E) very fine grained pyrrhotite and chalcopyrite filling interstitial space around pyroxene grains from DD10WOD004 (F) pyrrhotite, chalcopyrite and pentlandite in assemblage (this is a view of part of the area subject of a sulphide map (figure 11), from DD10WOD013 (G) pyrrhotite and chalcopyrite in assemblage, from DD10CAR011 (H) an area of pyroxene exsolutions, from DD10CAR011.

HARCUS

From within the Harcus intrusion four drill holes were chosen for more specific analysis with thin sections being made from intervals of chemical interest. The overall petrography for the Harcus intrusion, in addition to the mineral composition data, shows that the composition of the intrusion is far more iron rich than the Caroline intrusion. This can be seen in the summary ternary diagram of pyroxene compositions in figure 9 and suggests that the Harcus intrusion is sourced from a more fractionated melt. The textures that can be seen in the grain formation within the Harcus intrusion are that of sub-ophitic grain relationships with higher amounts of plagioclase able to be found within the cores at various different locations. In addition to this however there are isolated examples of cumulate textures within the intrusion also. From the presence of the sub-ophitic textures that have been noted, along with overall mineral geochemistry it is inferred that the Harcus intrusion is more representative of a melt that has then been captured and crystallised in place over some time than that of a traditional layered intrusions as could be said for the Caroline intrusion.

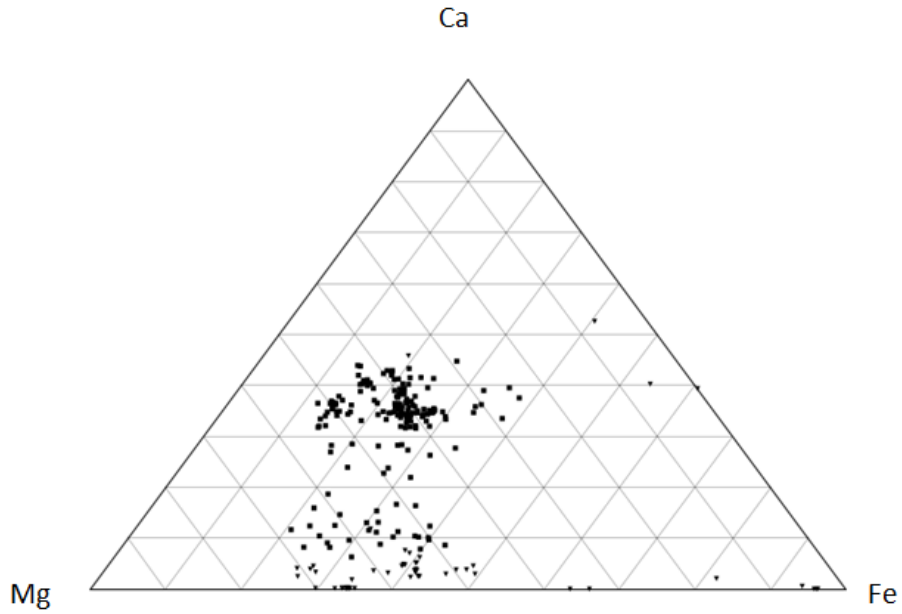

Figure 9 - summary ternary diagram of pyroxene compositions. Squares = CPX, triangles= OPX

The petrogenetic sequence of the Harcus intrusion were defined by standard petrographic methods; the textural relationships that can be seen in this intrusion suggest that pyroxene was the primary mineral that formed in this rock unit along with interstitial sulphide liquid which was then followed by the precipitation of the plagioclase units along with spinels and magnetite. Numerous different examples exist within this hole of re-equilibration of the different mafic minerals; specifically multiple interacting simplectites between pyroxenes, plagioclase and the sulphidic constituents, examples of this can be seen in figure 10e, 10f, 10i and 10j. In addition to the re-equilibration that could be seen occurring between the different silicate species, there was also evidence of infill and alteration that had taken place within sections of the core, as can be seen in figure 10c and 10d, and the breakdown of pyroxene (augite) grains to a finer grained amphibole (uralitic) species following the process suggested by Deer *et al.* (1966) possibly related to hydrothermal alteration of the intrusion, this can be seen in figure 10b and 10g.

The sulphides that were located within samples collected from the Harcus intrusion occurred as variably sized interstitial grains collected primarily around the pyroxene grains. From the observed textures of the sulphides it can be said that they formed as an initial MSS which then re-equilibrated to form the sulphide species of pyrrhotite, chalcopyrite and pentlandite. Of those sulphides the pyrrhotite is the most dominant of the three species present with chalcopyrite being less common and pentlandite only being found in isolated examples. Of note within some isolated examples of pyrrhotite and pentlandite is an unusual concentration of cobalt, with the highest example containing 8.5%w/w cobalt within a pentlandite grain.

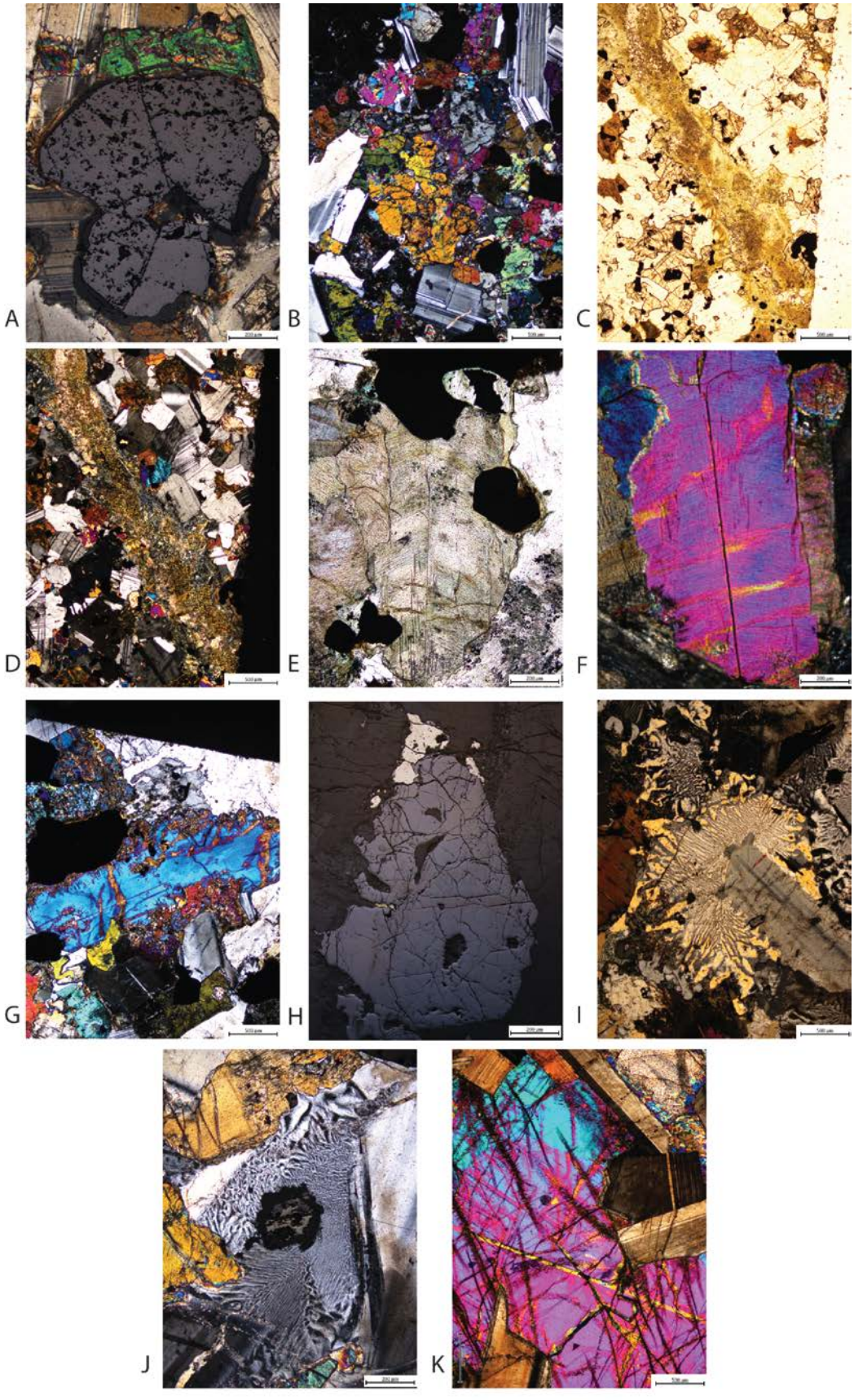
A
B
C
D
E
F
G
H
I
J
K

Figure 10 – (previous page) (a) a combined transmitted and reflected light image of an oxide grain, the surrounding silicates and the corona effects of chemical interaction between the two, from DD07HAR002 – 75m (b) an example of the suspected uralitic hornblende species from hydrothermal alteration, from DD07HAR002 – 150m (c) an example of a flow channel with infill, from DD07HAR002 -324m (d) an example of a flow channel with infill, from DD07HAR002 -324m (e) fine herring bone exsolution lamellae within pyroxene grains, from DD07HAR008 – 46m(f) fine herring bone exsolution lamellae within pyroxene grains, from DD07HAR008 – 46m (g) breakdown of pyroxene grains to finer grained products, from DD07HAR008 – 150m (h) an example of sulphides in assemblage, from DD07HAR008 – 338m (i) plagioclase and pyroxene simplectites, from DD07HAR009 – 101m (j) composite of transmitted and reflected light images of a very fine grained simplectites interaction between a sulphide assemblage, plagioclase and clinopyroxene, from DD07HAR009 – 101m (k) large grains of ortho- and clinopyroxene, from DD07HAR009 – 150m

Sulphide mapping

From the prepared thin sections, two examples were chosen for detailed mapping of the sulphide compositions on the microprobe. An example was taken from DD10WOD013 and D07HAR008 and shows in some detail the relationship of the three different sulphide species as they formed at thermodynamically stable points after crystallising as an initial MSS. The three main sulphide species that can be seen in the maps, figures 11 and 12, are those of pyrrhotite, chalcopyrite and pentlandite.

In each example it can be seen that there is an almost homogenous distribution of vanadium, manganese, chromium and titanium throughout the different sulphide species although in the example from the Harcus intrusion, figure 12, there are limited examples of exsolution structures in the upper right corner that show enhanced concentrations of titanium, vanadium and to a lesser extent manganese.

Within the Caroline examples map there does not appear to be any exsolutions of the metals of interest within the sulphide species.

When contrasting the two different sulphide maps it can be said that the concentrations recorded within the Caroline intrusion show higher concentrations in nickel than that of Harcus while the opposite can be said for copper concentrations, with the Harcus

intrusion having much higher concentrations of copper when compared to the Caroline intrusion.

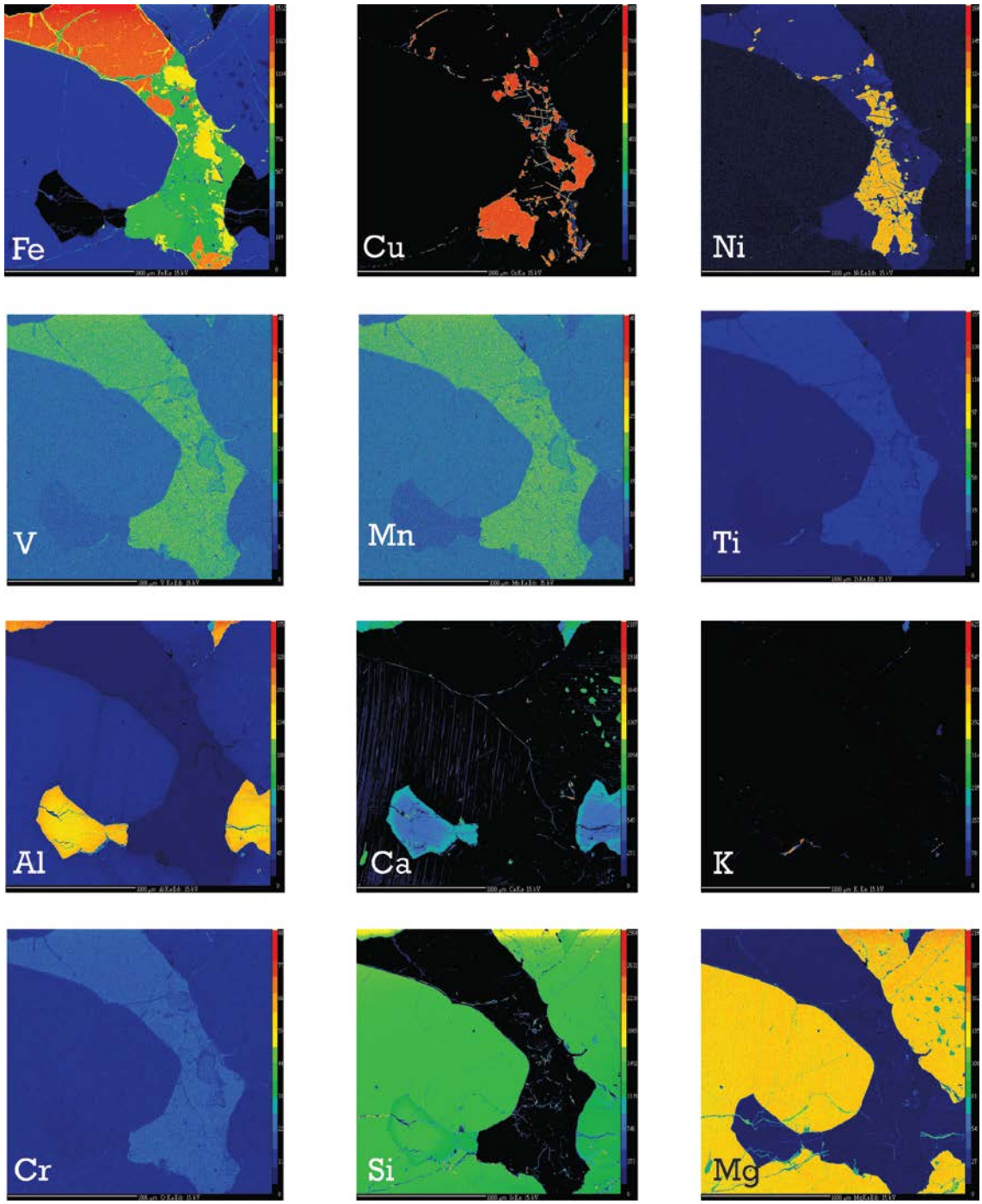

Figure 11 – colour representation of elemental abundances within a large sulphide assemblage, from drill hole DD10WOD013, at a depth of 100 meters.

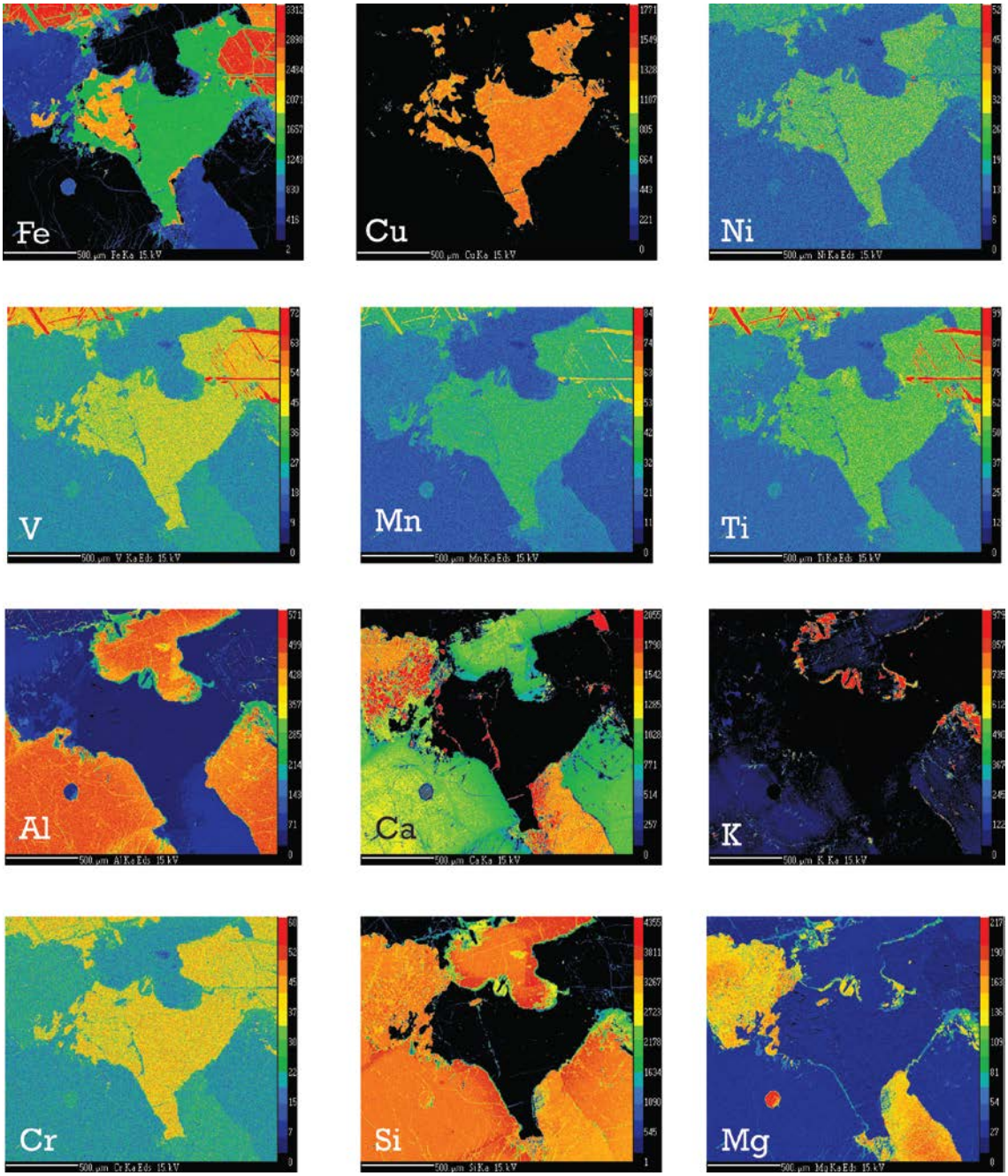

Figure 12 - a colour representation of elemental abundances within a large sulphide assemblage, from drill hole DD07HAR008, at a depth of 225 meters.

Whole Rock Minor and Trace Element Chemistry

From the analyses that were undertaken a full dataset of 37 elements was able to be obtained from a variety of holes at a range of depths across both the Harcus and Caroline intrusions. A full table of this data can be seen in table 3, 4 and 5.

Table 3 - Whole-Rock Trace Elements Data (Major elements in weight percent, minor and trace elements in ppm)

SAMPLE	BL1707	BL1708	DD07HAR001	DD07HAR001	DD07HAR002	DD07HAR002	DD07HAR008	DD07HAR008	DD07HAR008
DEPTH			80	170	75	324	46	150	370
NOTE	BLANK	BLANK							
SiO2 %	BDL	BDL	47	50	48	44	54	48	52
Al2O3 %	BDL	BDL	13	19	15	17	13	13	12
Fe2O3T%	BDL	BDL	18	7	17	15	15	18	9
MnO %	BDL	BDL	0	0	0	0	0	0	0
MgO %	BDL	BDL	6.55	8.65	6.01	8.49	3.02	5.93	12.29
CaO %	BDL	BDL	10.35	13.19	10.42	10.40	6.64	9.84	11.59
Na2O %	BDL	BDL	2.37	2.10	2.57	2.37	3.17	2.52	1.68
K2O %	BDL	BDL	0.60	0.23	0.66	0.29	2.07	0.82	0.41
TiO2 %	BDL	BDL	1.39	0.29	1.19	1.53	1.50	1.48	0.44
P2O5 %	BDL	BDL	0.10	0.07	0.11	0.16	0.26	0.13	0.09
SO3 %	BDL	BDL	0.08	0.05	0.07	0.07	0.09	0.07	0.10
LOI %	BDL	BDL	-0.47	0.31	-0.34	0.36	0.19	-0.09	0.21
Cu	BDL	NS	363.25	40.36	362.59	49.01	13.30	83.65	53.99
Co	NS	NS	160.00	54.95	82.18	91.57	60.26	68.20	47.43
Cr	NS	NS	3.81	181.11	3.76	83.82	1.79	3.56	1212.97
Ti	NS	NS	7080	1230	6053	7561	7797	6904	1973
Ba	BDL	BDL	257	91	274	144	823	322	163
Li	BDL	BDL	5	2	5	3	18	5	1
Sc	NS	BDL	42	22	38	21	30	36	18
Sr	BDL	BDL	187	179	210	288	191	182	122
V	NS	NS	630	109	565	225	230	513	177
Zn	BDL	BDL	86	27	76	85	90	88	42
Zr	NS	BDL	58	17	60	17	209	78	33
Pb	BDL	BDL	18	5	18	11	67	22	9
U		0.0017722	0.12	0.02	0.13	0.04	0.49	0.18	0.05
Th	NS	BDL	1.00	0.21	1.08	0.13	4.19	1.44	0.50
Rb	BDL	BDL	11.49	2.71	12.18	2.03	49.02	14.61	3.95
Nb	BDL	BDL	1.83	0.50	1.78	0.86	6.58	2.28	1.02
Cs	0.0064	BDL	0.07	0.08	0.09	0.09	0.48	0.12	0.01
Hf	NS	BDL	1.64	0.50	1.69	0.59	5.35	2.17	0.89
Ta	BDL	BDL	0.68	0.13	0.19	0.23	0.64	0.27	0.12
Tl	BDL	BDL	0.04	0.02	0.05	0.04	0.18	0.05	0.02
Y	NS	BDL	19.17	6.96	18.66	10.08	50.19	22.80	11.29
La	NS	BDL	8.83	2.65	9.35	3.59	33.07	11.75	6.39
Ce	BDL	BDL	18.97	5.84	20.01	8.12	71.43	25.47	13.86
Pr	NS	BDL	2.34	0.73	2.42	1.18	8.18	3.08	1.69
Nd	BDL	BDL	9.20	2.94	9.56	5.62	31.00	12.18	6.72
Sm	NS	NS	2.21	0.76	2.20	1.60	6.77	2.89	1.54
Eu	NS	NS	0.80	0.33	0.82	0.86	2.11	1.01	0.51
Gd	NS	BDL	2.79	0.96	2.77	1.87	7.76	3.53	1.82
Tb	NS	NS	0.50	0.18	0.49	0.31	1.34	0.61	0.31
Dy	NS	BDL	3.31	1.22	3.16	1.92	8.49	4.07	2.06
Ho	NS	NS	0.72	0.27	0.70	0.39	1.87	0.89	0.45
Er	NS	BDL	2.17	0.81	2.09	1.11	5.61	2.69	1.38
Tm	0.0098	NS	0.31	0.12	0.30	0.16	0.81	0.39	0.20
Yb	NS	NS	2.03	0.75	1.95	0.97	5.17	2.50	1.22
Lu	NS	NS	0.31	0.12	0.31	0.14	0.79	0.38	0.19
Sn	BDL	BDL	0.88	0.16	0.49	0.42	0.99	0.53	0.29

Table 4 –(Major elements in weight percent, minor and trace elements in ppm)

SAMPLE	DD07HAR009	DD07HAR009	DD10WOD002	DD10WOD002	DD10WOD002	DD10WOD002	DD10WOD003	DD10WOD003
DEPTH	150	150	67	110	150	150	65	85
NOTE	REPT	REPT			REPT	REPT		
SiO2 %	50		51	51	49		50	51
Al2O3 %	15		12	26	8		16	21
Fe2O3T %	10		12	3	13		8	6
MnO %	0		0	0	0		0	0
MgO %	9.16		16.42	4.41	21.77		10.50	6.83
CaO %	11.39		6.31	11.61	4.83		12.14	9.80
Na2O %	2.16		1.64	3.23	0.74		2.20	2.97
K2O %	0.43		0.26	0.23	0.04		0.23	0.47
TiO2 %	0.54		0.38	0.11	0.20		0.45	0.22
P2O5 %	0.09		0.04	0.04	0.02		0.06	0.05
SO3 %	0.07		0.05	0.07	0.12		0.06	0.09
LOI %	0.17		0.25	0.38	0.82		0.52	1.54
Cu	82.30	82.74	204.39	34.95	202.80	205.93	54.30	249.00
Co	57.80	58.81	99.84	51.04	258.83	253.63	68.55	60.86
Cr	63.14	62.80	781.46	188.70	1445.50	1467.52	240.12	122.76
Ti	2396	2469	1790	429	936	924	2108	1095
Ba	177	170	113	75	13	13	82	119
Li	3	2	1	1	1	1	2	3
Sc	31	25	5	5	8	8	29	12
Sr	185	173	124	308	51	49	175	277
V	187	187	170	37	163	160	185	92
Zn	50	49	65	9	52	50	32	34
Zr	36	31	14	2	4	4	18	6
Pb	11	10	8	3	19	18	4	8
U	0.07	0.07	0.03	0.01	0.01	0.01	0.03	0.02
Th	0.54	0.47	0.07	0.02	0.01	0.01	0.07	0.06
Rb	7.28	6.13	0.88	0.89	0.34	0.32	1.72	2.05
Nb	1.22	1.23	0.45	0.09	0.06	0.06	0.32	0.28
Cs	0.17	0.08	0.01	0.01	0.01	0.01	0.02	0.03
Hf	0.95	0.82	0.47	0.08	0.15	0.16	0.62	0.23
Ta	0.12	0.13	0.21	0.21	0.55	0.55	0.22	0.25
Tl	0.03	0.03	0.02	BDL	0.02	0.02	0.02	0.04
Y	13.85	12.85	5.19	1.01	3.02	2.98	9.35	3.14
La	6.46	6.12	2.33	0.93	0.32	0.30	2.17	1.62
Ce	14.10	13.28	4.85	1.72	0.75	0.73	5.79	3.31
Pr	1.72	1.63	0.62	0.20	0.12	0.11	0.88	0.42
Nd	6.78	6.52	2.59	0.75	0.60	0.58	4.16	1.69
Sm	1.61	1.58	0.68	0.17	0.22	0.21	1.21	0.43
Eu	0.57	0.54	0.37	0.25	0.12	0.12	0.49	0.37
Gd	2.05	1.90	0.87	0.17	0.38	0.36	1.58	0.52
Tb	0.36	0.35	0.17	0.03	0.08	0.08	0.28	0.10
Dy	2.41	2.26	1.05	0.19	0.57	0.54	1.78	0.57
Ho	0.53	0.51	0.24	0.05	0.14	0.13	0.38	0.14
Er	1.62	1.58	0.74	0.13	0.43	0.43	1.09	0.40
Tm	0.24	0.22	0.12	0.03	0.07	0.07	0.17	0.07
Yb	1.55	1.48	0.76	0.14	0.47	0.46	1.01	0.41
Lu	0.23	0.22	0.12	0.03	0.08	0.08	0.16	0.07
Sn	0.44	0.47	2.84	0.43	1.27	1.17	2.71	1.03

Table 5 –(Major elements in weight percent, minor and trace elements in ppm)

SAMPLE	DD10WOD004	DD10WOD004	DD10WOD013	DD10WOD013	DD10CAR011	DD10CAR011
DEPTH	190	220	100	125	230	305
NOTE						
SiO2 %	45	49	50	45	50	51
Al2O3 %	11	7	13	13	11	9
Fe2O3T %	17	14	10	20	12	14
MnO %	0	0	0	0	0	0
MgO %	13.74	22.12	15.17	7.20	15.99	17.93
CaO %	8.57	3.42	9.03	9.98	6.92	7.02
Na2O %	1.30	0.57	1.38	2.46	1.53	1.13
K2O %	0.10	0.07	0.09	0.30	0.16	0.12
TiO2 %	0.30	0.27	0.21	2.17	0.37	0.38
P2O5 %	0.04	0.02	0.03	0.05	0.04	0.03
SO3 %	0.15	0.13	0.10	0.08	0.07	0.07
LOI %	1.13	0.09	0.24	-0.15	-0.10	0.46
Cu	1379.14	283.13	694.23	185.24	101.86	188.74
Co	231.32	173.50	131.06	145.45	367.84	110.52
Cr	1063.93	1254.62	417.80	102.61	619.89	851.52
Ti	1319	1134	892	10495	1656	1802
Ba	35	29	25	98	61	44
Li	1	1	1	2	1	1
Sc	26	13	16	28	3	6
Sr	102	36	113	176	136	96
V	173	161	151	786	161	191
Zn	46	61	39	92	66	68
Zr	9	7	4	19	12	10
Pb	31	12	8	6	5	5
U	0.01	0.01	0.01	0.02	0.01	0.01
Th	0.03	0.03	0.02	0.08	0.02	0.01
Rb	0.93	0.94	0.36	1.53	0.43	0.29
Nb	0.21	0.18	0.13	0.98	0.06	0.11
Cs	BDL	0.01	0.02	0.01	BDL	BDL
Hf	0.33	0.23	0.17	0.73	0.40	0.38
Ta	0.22	0.35	0.26	0.37	0.64	0.15
Tl	0.02	0.03	BDL	BDL	BDL	BDL
Y	5.24	3.54	3.62	10.80	5.35	5.90
La	0.92	0.73	0.48	1.70	1.39	1.10
Ce	2.25	1.50	1.20	4.43	3.46	2.83
Pr	0.33	0.20	0.18	0.68	0.51	0.44
Nd	1.58	0.86	0.88	3.35	2.41	2.20
Sm	0.51	0.27	0.32	1.09	0.71	0.69
Eu	0.24	0.12	0.18	0.53	0.29	0.28
Gd	0.74	0.42	0.50	1.60	0.89	0.92
Tb	0.14	0.08	0.09	0.30	0.16	0.17
Dy	0.95	0.59	0.65	1.95	1.09	1.12
Ho	0.21	0.14	0.14	0.42	0.24	0.26
Er	0.65	0.47	0.47	1.25	0.74	0.82
Tm	0.09	0.08	0.07	0.18	0.11	0.11
Yb	0.59	0.54	0.47	1.15	0.69	0.78
Lu	0.10	0.09	0.07	0.17	0.11	0.12
Sn	2.59	2.36	0.61	0.48	1.21	1.69

CAROLINE

The Caroline intrusion geochemical signatures have relatively flat REE patterns when using chondritic normalisation using values from McDonough and Sun (1995) and when being scrutinised in the form of a trace element diagram using the primordial melt from McDonough *et al.* (1992) the pattern is highly variable. The overall trend in the rare earth pattern is that of enrichment in the elements in a uniform manner from 1.5 chondrite norm up to 10 times chondrite norm. The trace element trends shows enrichment in barium, tantalum, strontium and lead whilst also containing depletions in caesium, thorium, niobium and zirconium. The high concentrations in lead is believed to not be an error as this is consistent with other data collected from within the Giles complex intrusions (Seat *et al.* 2011). The geochemical signature for these trace elements is remarkably similar across the different drill holes and depths with the only variability coming from the amount that the signature is moved up or down relative to the chondritic norm. The geochemical trends for both trace elements and rare earth elements can be seen in figure 13a.

Of note within the rare earth element patterns for the Caroline intrusion are the different patterns that can be seen in the drill hole DD10WODO002. There are distinctly different patterns that can be seen between the different depths. It is believed that the low HREE concentrations and enrichment in LREE is a signature that has been caused by the high amounts of plagioclase that has been formed in the section of the core that has been selected. The rare earth pattern in question can be seen in figure 13b.

A

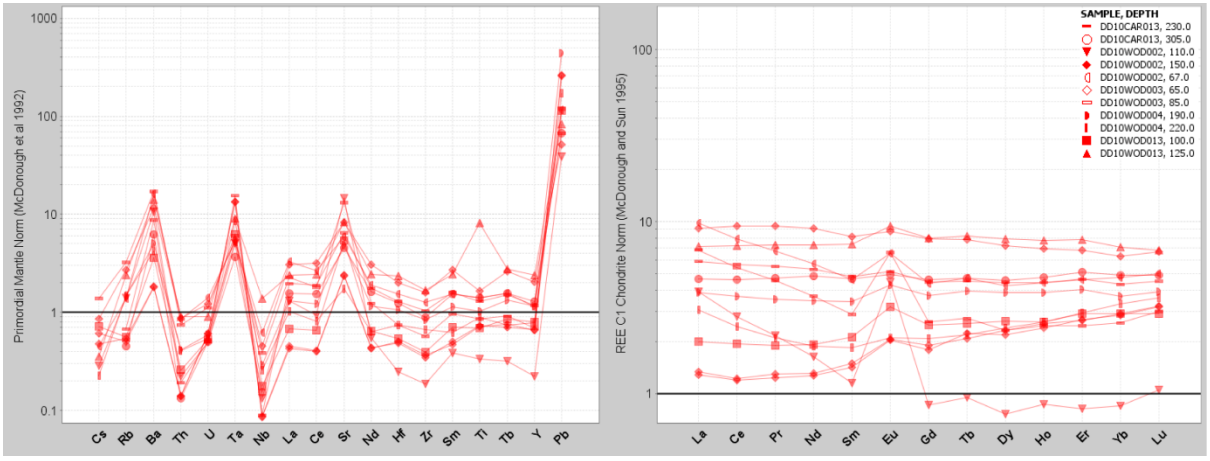

B

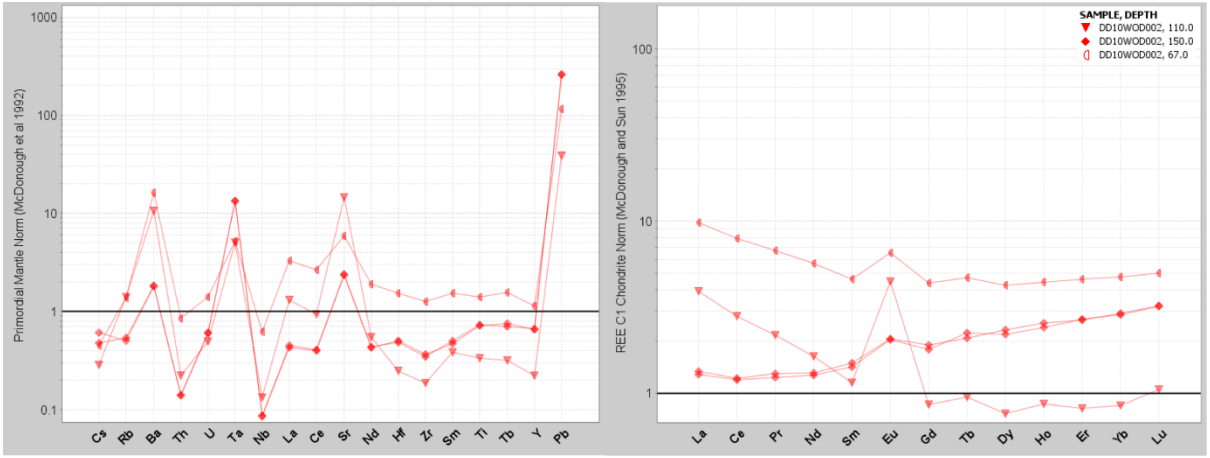

Figure 13 - trace element and rare earth element diagrams of all Caroline intrusion data (a), and DD10WOD002 (b). Rare earth and trace element diagrams are normalised using values from McDonough and Sun (1995)

HARCUS

The Harcus intrusion gave an overall geochemical trend that contrasts that of the Caroline intrusion. The REE patterns when normalised to chondrite gave values from five times chondritic norm through to in excess of 100 times. In almost all cases the Harcus drill hole samples gave a pattern that was more highly enriched in LREE, decreasing across the series through to samarium where upon the pattern generally remained flat. Some sample intervals contained anomalies in enrichment in europium. The trace element plots for the Harcus intrusion data shows enrichment in almost all of the elements being examined with relatively large degrees of enrichment able to be found in barium, lanthanum, neodymium and lead. The relative low concentrations within the Harcus data are those of thorium, uranium, niobium, zirconium and titanium. The trace element and REE plots of the Harcus data can be seen in figure 14.

The different trends that can be seen in both the trace element and rare earth element plots is believed to be the product of varying levels of fractionation in the in the crystallising melt. This is supported by the consistent pattern across the different drill holes and depths within the intrusion with the only major variation coming in the form of consistent changes across the entire suite of elements.

The europium enrichment that can be seen within the different REE plots is believed to be the product of higher levels of plagioclase precipitation within those sections of the intrusion.

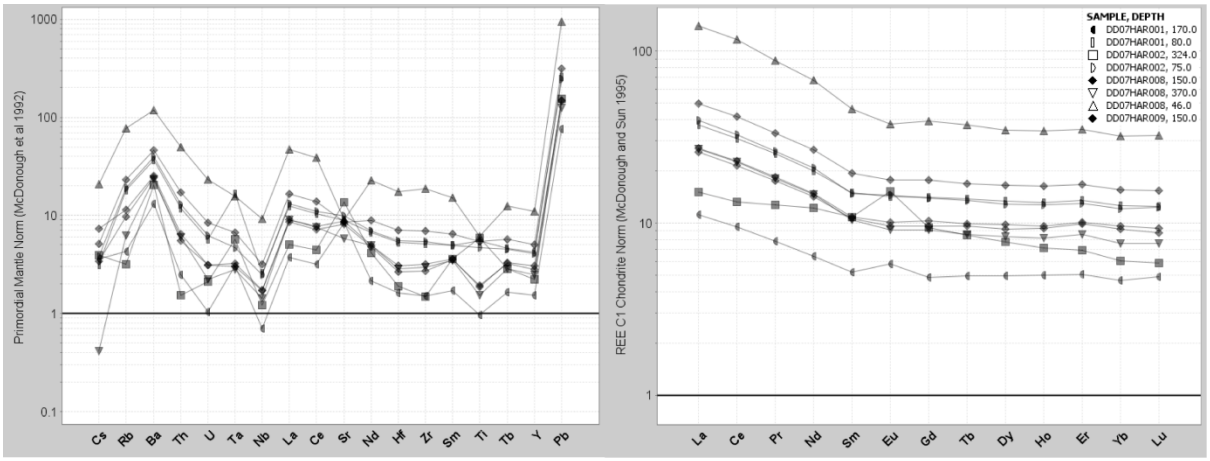

Figure 14 - trace element and rare earth element diagrams of all data from that Harcus intrusion, Rare earth and trace element diagrams are normalised using values from McDonough and Sun (1995)

Nd-Sm-Sr

The Nd-Sm-Sr isotopic ratios were determined from the 6 samples that were collected. These gave a mean εNd(total) of -2.69 for the Caroline intrusion and -1.18 for the Harcus intrusion. The results of this analysis can be seen in table 6 and represented in εNd format in figure 15.

Table 6 –Results from the Nd-Sr-Sm isotope analysis

Sample	WOD013 - 41.6	WOD013 - 80	HAR008 - 46	HAR008 - 150	HAR008 - 278	HAR008 - 370
87/86Sr	0.706727	0.707759	0.7164132	0.7085947	0.7077921	0.7071252
2 se (x1E-6)	*10.4*	*10.9*	*11.2*	*9.8*	*12.3*	*12.3*
input age of rock T (Ma)	*1070.0*	*1070.0*	*1070.0*	*1070.0*	*1070.0*	*1070.0*
Unmixed 143/144Nd	.512142	*.512463*	*.512099*	*.512168*	*.512181*	*.512127*
147Sm/144Nd	*.1476*	*.1891*	*.1280*	*.1386*	*.1401*	*.1325*
εNd (T=0)	*-9.68*	*-3.42*	*-10.51*	*-9.16*	*-8.91*	*-9.97*
143Nd/144Nd (T)	*0.51110499*	*0.51113475*	*0.51120004*	*0.51119492*	*0.51119758*	*0.51119622*
εNd (T)	-2.98116241	-2.3991275	-1.1220202	-1.22216908	-1.17028668	-1.19682611

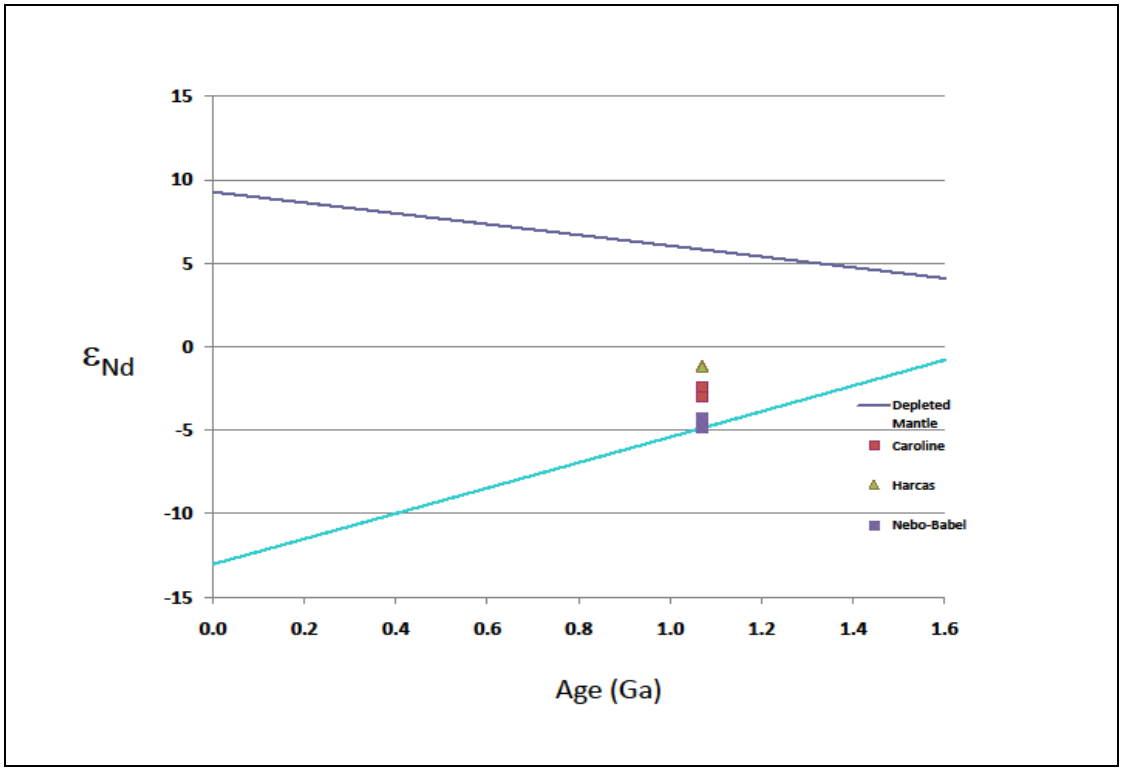

Figure 15 - εNd diagram of the Caroline and Harcus intrusions. The Nebo-Babel intrusion has been included for reference (Godel *et al.* 2011).

Using this data in connection with the whole rock chemical dataset it was possible to determine isotope ratios for the different components and thus determine the level of crustal assimilation within the two different intrusions. The graph representing this can be seen below. From this it was possible to define that the Harcus intrusion had undergone 15% crustal assimilation and the Caroline had undergone 35% crustal assimilation. This can be seen below in figure 16 which shows the curve of isotopic mixing at the time of intrusion from which the relative amount of assimilation was able to be determined.

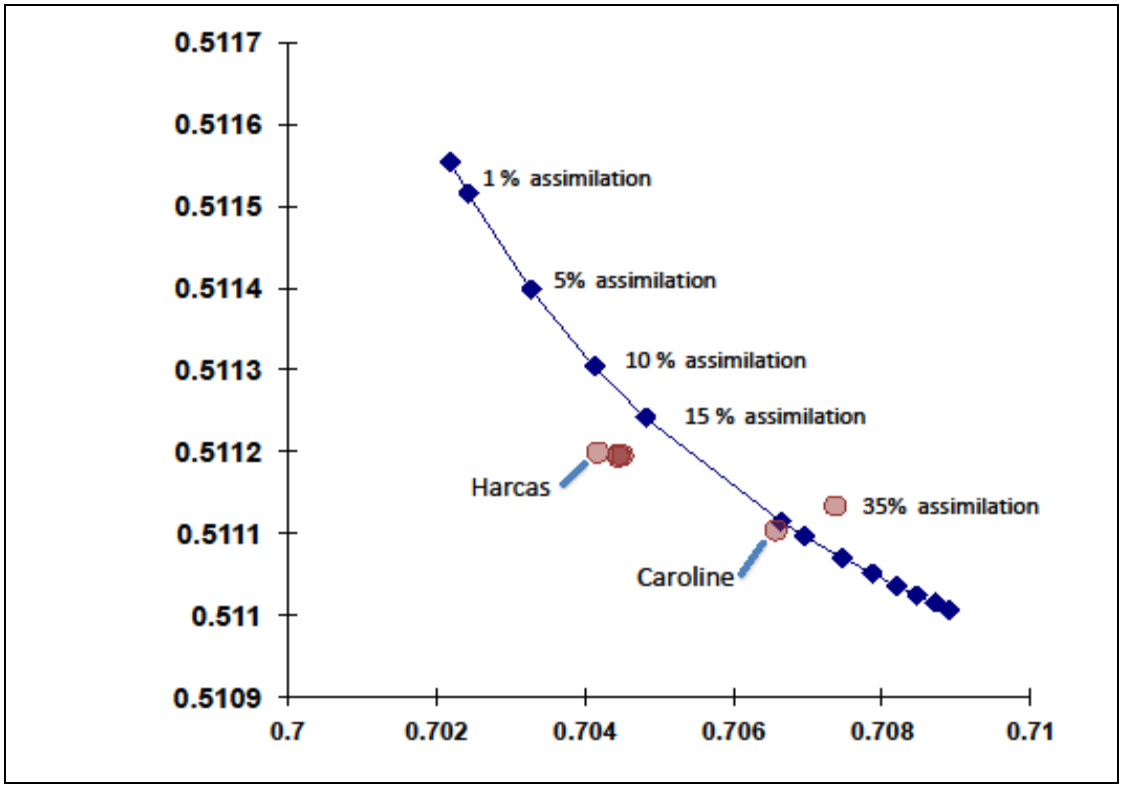

Figure 16 - isotope mixing diagram of MORB and Orthogneiss country rock from Godel *et al.* (2011)

DISCUSSION

It was possible to determine the pressure and temperature of the two different intrusions as the different minerals of interest were crystallising out of the bulk melt by process of pyroxene thermobarometry. This was done using the methods of two pyroxene thermobarometry as defined by Putirka (2008) and clinopyroxene barometry as defined by Nimis and Taylor (2000). From the various different methods of barometry a selection of different pressures where determined with a mean of 3.8 – 4.2 kBar for both the Harcus and Caroline intrusions. The full selection of pressures as determined can be seen in table 7.

Table 7 - calculated temperatures and pressures acquired through the combined process of two pyroxene thermometry (Putirka 2008) and clinopyroxene barometry (Nimis & Taylor 2000). For examples where two-pyroxene thermometry was not possible an iterative process was undertaken to with constraints on the temperatures used to keep them within the range of spatially related data points.

Intrusion	Hole ID	Depth (m)	Mean Calculated Temperature (°C)	n	Standard deviation (°C)	Temperature used for geobarometry (°C)	% difference	Mean Calculated Pressure (kBar)	n	Standard Deviation (kBar)
Harcus	*DD07HAR001*	**80**	***1099.9***	3	7.8	1050	-4.536776071	3.85	2	1.71
		150	**-**	-	-	1100	ESTIMATED THROUGH ITERATION	4.93	15	1.58
	DD07HAR002	**225**	***1321.4***	14	25.2	1150	-12.97109127	3.97	8	1.71
		324	***1068***	17	95.7	1068	0	2.94	2	0.81
	DD07HAR008	**225**	***1110***	20	52	1000	-9.90990991	3.47	6	1.05
		300	***1130.2***	15	62.6	1130	-0.017695983	5.29	12	1.31
	DD07HAR009	**150**	***1250***	3	58.9	1300	+4	5.97	12	2.34
		260	***1145***	2	9	1100	-3.930131004	3.8	7	2.33
Caroline	*DD10CAR011*	**230**	***1060***	183	52	1060	0	4.75	22	0.67
		240	***1012***	69	51.6	1012	0	2.93	10	1.33
		305	***1038***	52	43.1	1038	0	4.41	8	0.78
		310	***970***	10	22.5	970	0	2.57	15	0.83
	DD10WOD002	**45**	***1025***	36	42	1250	+21.95121951	4.66	17	0.71
		67	**-**	-	-	1100	ESTIMATED THROUGH ITERATION	6.31	2	0.41
		110	***904***	499	64	1025	+13.38495575	3.7	23	1.25
		130	***987***	59	60.6	1300	+31.71225937	3.25	9	1.56
		135	***993.4***	203	50.9	1250	+25.83048118	3.62	7	0.78
		150	***995.7***	287	65.1	1250	+25.53982123	3.23	15	1.1
		153	***1040***	2	202	1040	0	3.22	8	0.79
	DD10WOD003	**65**	***1001***	67	38.8	1025	+2.397602398	3.93	20	0.86
		75	**-**	-	-	1025	ESTIMATED THROUGH ITERATION	3.66	5	0.56
	DD10WOD004	**190**	***1048***	16	75.8	1200	+14.50381679	4.6	11	1.9
		215	**-**	-	-	1050	ESTIMATED THROUGH ITERATION	4.3	30	0.707
		220	***1125***	19	34.6	1125	0	4.6	5	0.82
	DD10WOD013	**100**	**-**	-	-	1100	ESTIMATED THROUGH ITERATION	3.53	10	1.02
		104	**-**	-	-	1050	ESTIMATED THROUGH ITERATION	3.35	6	0.88
		125	***1049.5***	8	92.7	1050	+0.047641734	3.3	17	1.55

From data that was made available by Pepininni minerals (Rutherford & Clifford 2008, Rutherford 2010, 2011) investigations into the trends of nickel, copper and sulphur concentrations were able to be investigated with the aim of determining the different trends within the two intrusions.

Between the two different intrusions there are distinctly different patterns that emerge showing the contrast between the two. The trends that can be seen within the Caroline intrusion (figure 17a, 17c and 17e) are those of early accumulation (high magnesium number) of high concentrations of all three elements being scrutinised with this then dropping off quickly when moving to lower magnesium numbers. When considering the Harcus intrusion (figure 17b, 17d and 17f) the trend that is found in the Caroline intrusion is not present, there is a trend that suggests a more consistent and melt like composition that then continues across the range of magnesium numbers. In addition to this there is a large anomaly in copper and sulphur concentrations at relatively evolved magnesium numbers, 20-30. This is also present, but to a lesser extent, in the nickel concentrations for the Harcus intrusion. This may be due to a change in the different precipitating minerals and in turn a change in the redox state of the melt and a change in the metal content in the minerals being precipitated at the time. This may also be zones where conditions may have been appropriate for depleted sulphide precipitation.

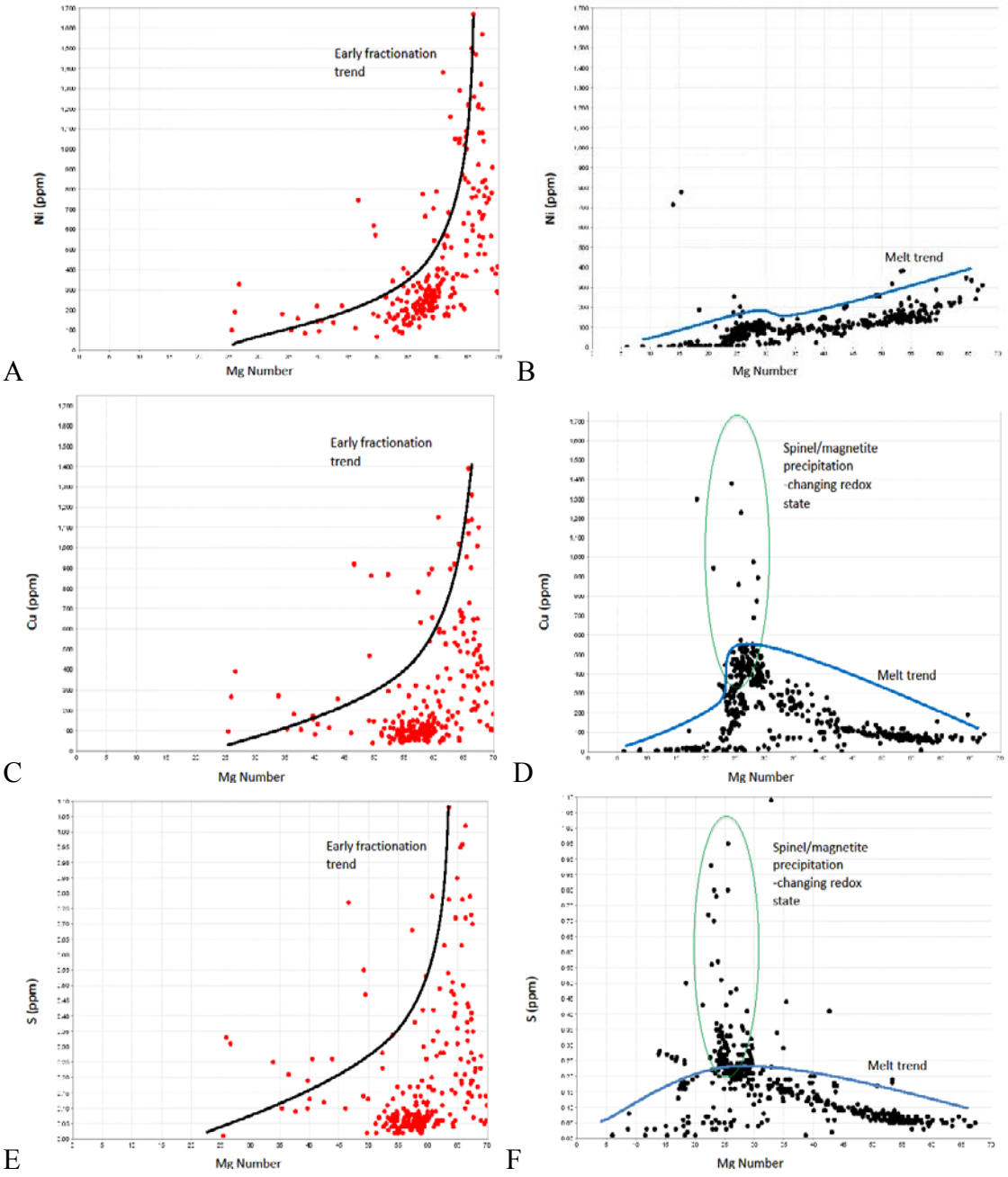

Figure 17 – (a) annotated graph of magnesium number against nickel concentrations in the Caroline intrusion (a) annotated graph of magnesium number against nickel concentrations in the Harcus intrusion(a) annotated graph of magnesium number against copper concentrations in the Caroline intrusion(a) annotated graph of magnesium number against copper concentrations in the Harcus intrusion(a) annotated graph of magnesium number against sulphur concentrations in the Caroline intrusion(a) annotated graph of magnesium number against sulphur concentrations in the Caroline intrusion. Data from core composite whole rock data from Rutherford and Clifford (2008), Rutherford (2010, 2011).

From the whole rock data that was collected in this study it was possible to define a possible model composition for the parental melt for both the Caroline and Harcus intrusions. This was done with a starting composition from Godel *et al.* (2011) which was then optimised to fit the trends that were presented by the whole rock data.
The model melt was subjected to iterative crystallisation modelling using the MELTS software based upon the work of Ghiorso and Sack (1995). The different testing conditions were undertaken in order to understand the different conditions that may have played a role in the evolution of the melt as it crystallised. The starting composition for the model melt can be seen below in table 8.

Table 8 - Major element compositions in percent weight of oxides of model melt for both suites of intrusions

Major element	% oxide
SiO_2	50.51
TiO_2	0.84
Al_2O_3	13.67
Fe_2O_3	2.17
Cr_2O_3	0.03
FeO	8.07
MnO	0.19
MgO	11.82
NiO	0.01
CaO	10.11
Na_2O	1.94
K_2O	0.46
P_2O_5	0.07
H_2O	0.1

The simulation was able to model the melts from their liquidus temperature through to approximately 1000 °C. The purpose of the crystallisation simulation was to best represent the assemblages of minerals and compositions that could be found within the Caroline intrusion whilst also being able to track the melt like trend of the Harcus intrusion.

The redox state of the composition before crystallisation was calculated using the known quartz-fayalite-magnetite buffering system; the calculations for fractional crystallisation however were not subject to the same buffering as they were assumed to be in a closed system. The pressure that was finally chosen as the ideal one for the modelled system was that of 3.5 kbar. This was chosen as at higher pressures the primary Fe-Mg phase became that of garnet, and at lower pressures olivine became a more dominant phase.

The evolution of the different major elements and the trends that they follow can be seen below in figure 18 and 19. When observing this it can be seen that the Harcus intrusion tracks with some degree of accuracy to the composition of the melt, confirming the assumption that it is more of a captured melt than a layered intrusion like that of Caroline. This leads to the conclusion that the Harcus intrusion may have already been through a phase of crystallisation and fractionation before it was finally emplaced in its current location

The different mineral compositional fields have been placed on the figures and show the location of the mineral geochemical fields as determined on the microprobe in addition to the whole rock data for both the Caroline and Harcus intrusion. From these representations it is possible to see where the different precipitating minerals have driven the melt during its evolution and this also confirms the petrography that was undertaken, supporting the petrogenetic model suggesting initial precipitation of orthopyroxene, followed by clinopyroxene with minor spinels followed by the precipitation of plagioclase.

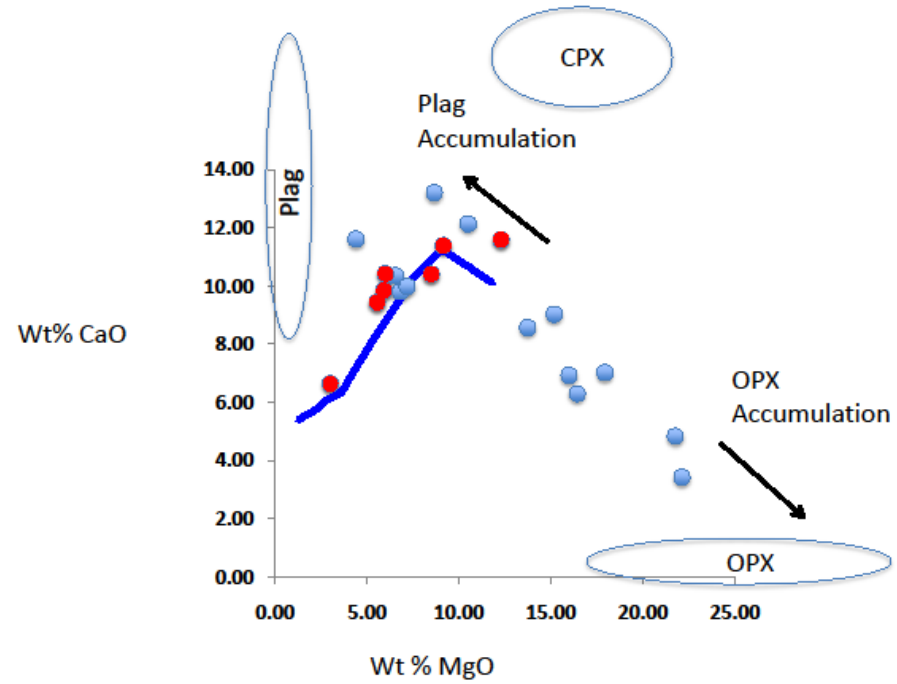

A

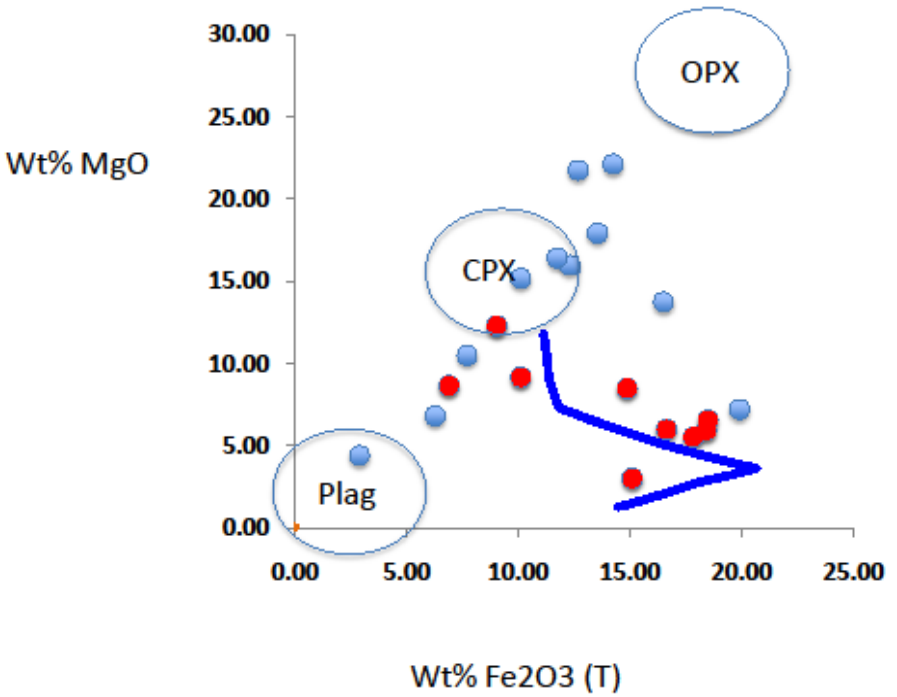

B

Figure 18 – (a) CaO Wt% v MgO Wt% with whole rock data (Caroline blue, Harcus red), mineral compositional zones from microprobe work highlighted and the modelled melt evolution plotted (blue line) (b) MgO Wt% v Fe_2O_3 Wt% with whole rock data (Caroline blue, Harcus red), mineral compositional zones from microprobe work highlighted and the modelled melt evolution plotted (blue line)

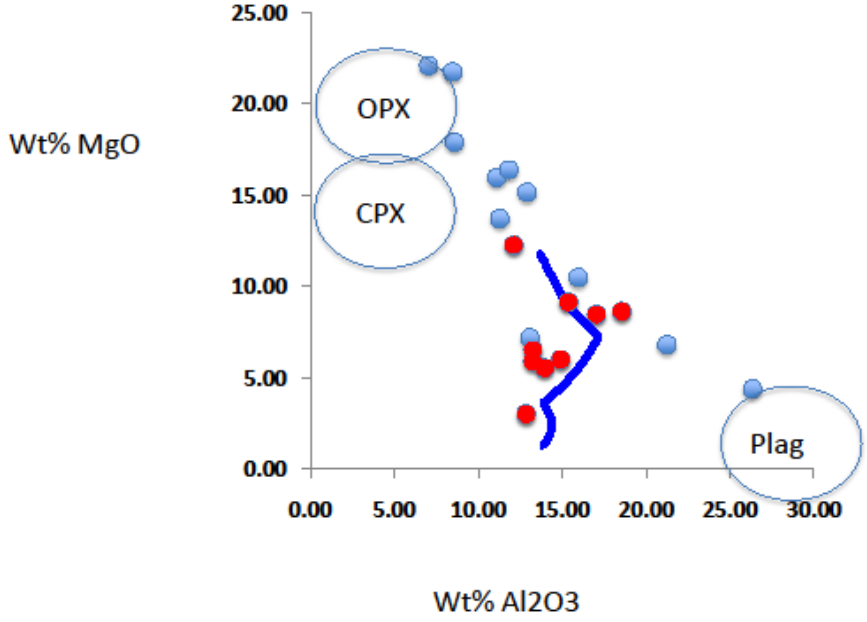

A

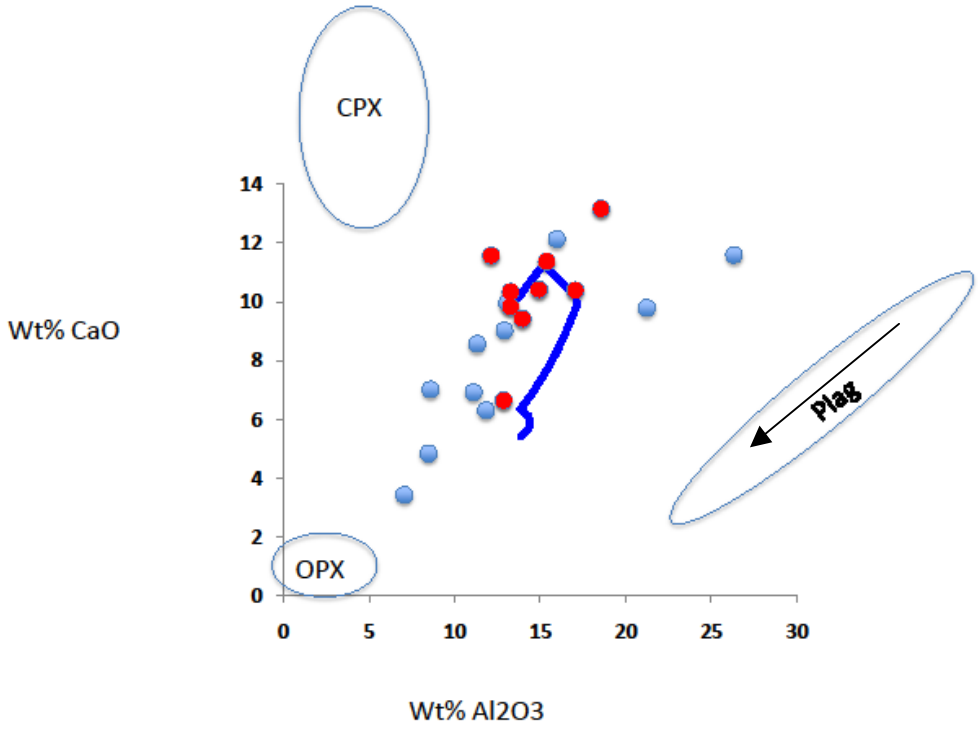

B

Figure 19 – (a) MgO Wt% v Al_2O_3 Wt% with whole rock data (Caroline blue, Harcus red), mineral compositional zones from microprobe work highlighted and the modelled melt evolution plotted (blue line) (b) CaO Wt% v Al_2O_3 Wt% with whole rock data (Caroline blue, Harcus red), mineral compositional zones from microprobe work highlighted and the modelled melt evolution plotted (blue line). The plagioclase compositions in these samples existed over a large field that began as high CaO and high Al_2O_3 and moved to lower values over the course of the crystallisation sequence as indicated.

Using the model that was defined it was possible to determine the Fe2+ and Fe3+ ratios for each point that was modelled through temperature space, this can be seen in figure 20.

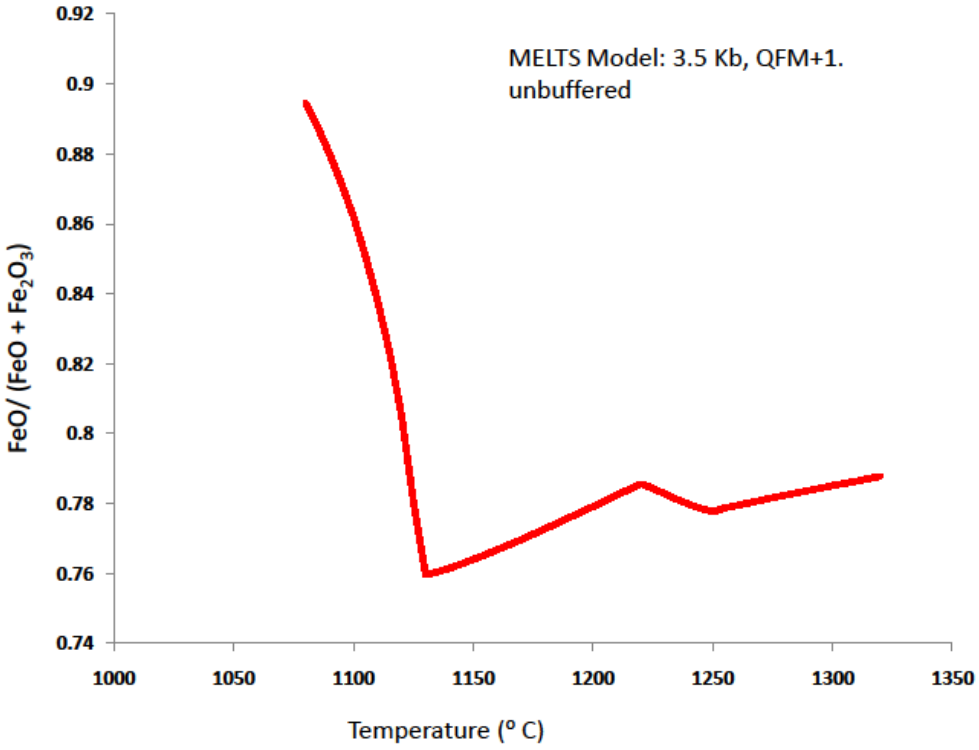

Figure 20 - FeO/ (FeO + Fe2O3) against temperature using values calculated from the MELTS model through temperature space

Using this information, in addition to the temperatures and pressures determined previously it was then possible to calculate the sulphur concentration at sulphide saturation by using the formulas defined in Liu *et al.* (2007). In addition to this, the sulphur fractionation curve in the absence of sulphur saturation was also calculated for the model and was found to be similar to that of K_2O. This was then combined with the defined sulphur saturation curve to give a point in temperature and sulphur concentration space where the sulphur would have come out of the silicate melt and formed into an immiscible liquid that would have then settled with the precipitating

minerals due to the density differences. This can be seen in figure 21 and shows that the sulphide saturation would have occurred at an early point at approximately 1250°C.

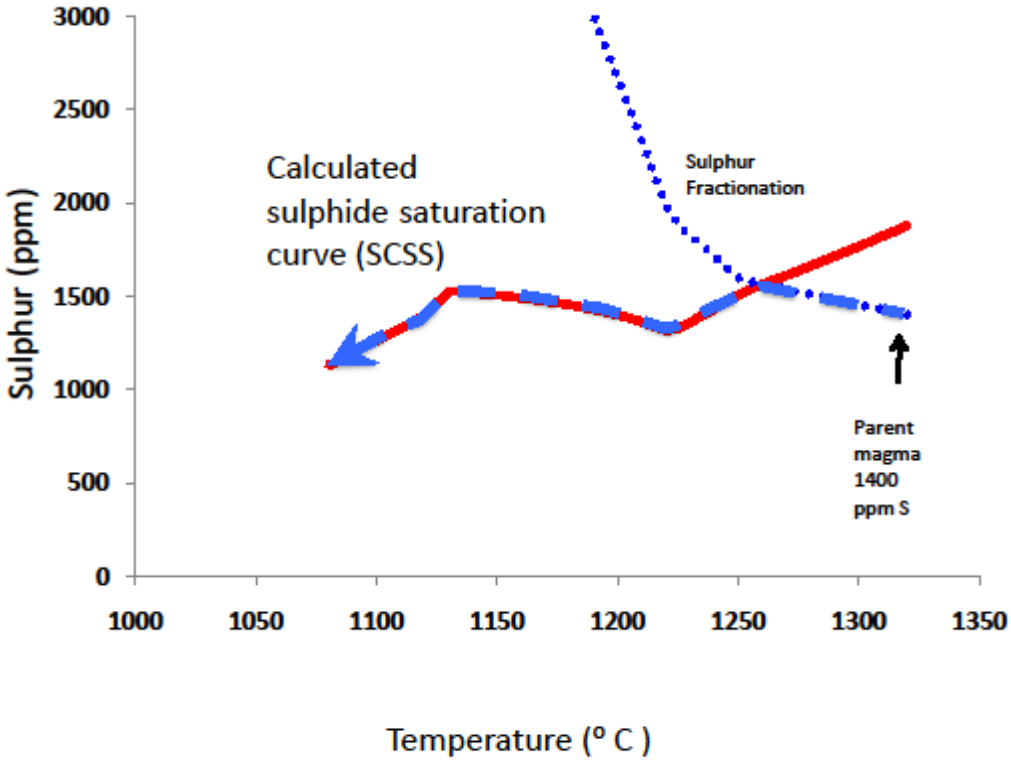

Figure 21 - The calculated Sulphide saturation curve (SCSS) through temperature space with the sulphide fractionation curve also represented with its intersection with the SCSS

Using this temperature it is possible to then use the MELTS model to determine which minerals where precipitating at the time when the saturation event occurs. At this time the minerals that were precipitating according to the model were those of orthopyroxene and minor amounts of clinopyroxene, this can be seen in figure 22 which shows the evolution of the different phases in the melt through the range of temperatures scrutinised.

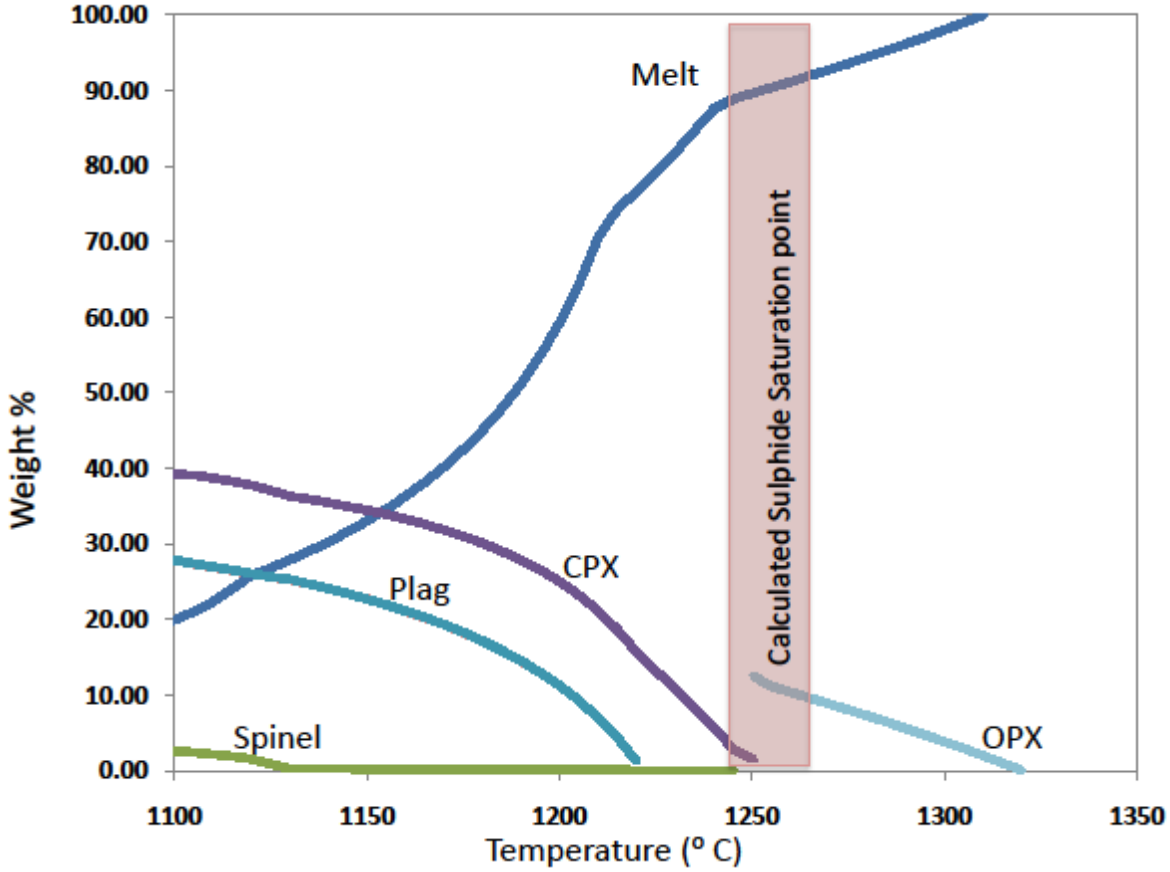

Figure 22 - The abundances of the different phases as they crystallised over the range of temperatures with the sulphide saturation point highlighted.

When considering the evolution of the magmas from which the two intrusions are formed the Nd-Sr isotopic ratios show us that differing degrees of assimilation of crustal material has taken place, 35% for Caroline and 15% for Harcus. Using this information it is then possible to say that the magmas for both intrusions must have experienced at least two stages of ponding in the crust to allow for the assimilation of country rock material. The depth at which this ponding and assimilation has taken place is not able to be constrained at this point but it is reasonable to presume that it has occurred at a lower crustal level to the point at which the intrusions were then emplaced.

From the afore mentioned details relating to the two intrusions and their different evolutions, the geochemical data suggests that evolution of the magma is that the Caroline intrusion is, although showing more crustal contamination, is less evolved that that of the Harcus intrusion. The Harcus intrusion is more representative of a melt that may have been transported away from a crystallising layered intrusion such as the Caroline intrusion. This is supported by the textures that can be seen at both the core level, thin section and the consistency of the modelled melt with the two different intrusions in their own different ways, the Caroline is more representative of the crystallisation products while the Harcus is more representative of the melt that is remaining as it evolves.

With that in mind it can be said that the Harcus intrusion has already undergone a period of fractional crystallisation and then the resultant residue has then moved on to form the current intrusion. The correlation between the high magnesium number minerals and their associated high sulphur contents suggests that the precipitation of the sulphide phase within the Harcus intrusion has already occurred at least once in the evolution of the melt before emplacement. This is supported by the concentrations of the different metals within the assemblages of sulphides found within the Harcus and Caroline intrusions. The higher concentrations of nickel with lower concentrations of copper of the Caroline intrusion when compared to the Harcus (which contains much higher concentrations of copper but half the concentrations of nickel) suggests that an early phase of accumulation of either a silicate phase or a sulphide phase as previously discussed may have taken place causing the change in concentration of the metals in question. A possible model for the evolution of the magmas through the crust can be seen in figure 23.

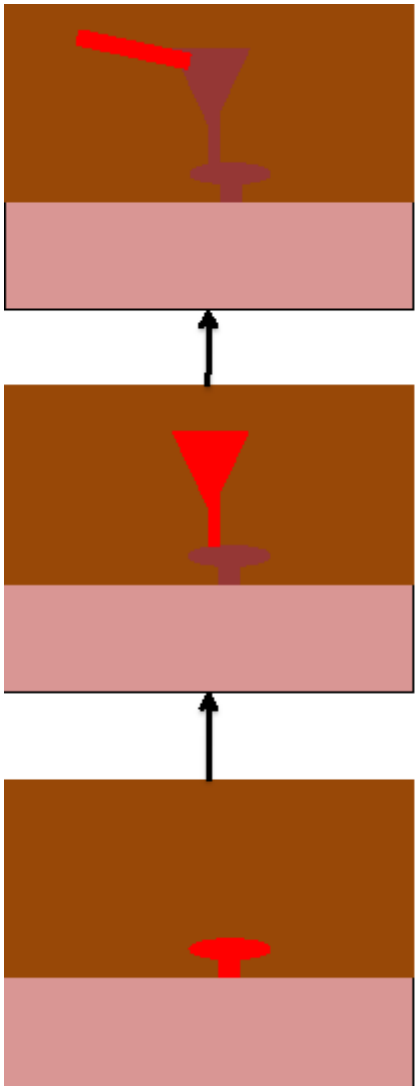

Figure 23 - a basic diagram showing an emplacement model for the two intrusions

CONCLUSIONS

From the mineral analyses that have been undertaken in this study it is possible to show that the two Giles complex intrusions formed at 3.8 kbar – 4.2 kbar. In addition to this, using the εNd values for the samples from each intrusion it is possible to say that not only did the two intrusions have the assimilation of crustal material in their genesis but they had each done so in differing amounts. It was determined that the Harcus intrusion has experienced 15% crustal assimilation in its evolution and the Caroline intrusion has

experienced 35% crustal assimilation in its evolution. Using the data from Pepininni Minerals an early accumulation trend for sulphur; copper and nickel was noted in the Caroline and a late trend with a more melt like composition in the Harcus. This was then confirmed with the model that was defined and then tested with crystallisation simulations. This model composition was found to be an appropriate match to both intrusions with the Caroline intrusion matching the crystallising products of the simulation and the Harcus intrusion matching the path of the melt evolution confirming the assumption that the Harcus intrusion is better described as a trapped melt than a layered intrusion. From the simulation it was possible to define the redox state of the melt through time and from this the sulphur content at sulphur saturation, this was mapped through temperature space and an appropriate temperature condition for the initial sulphide phase to separate as an immiscible liquid was found to be approximately 1250^{o}C. When comparing this to the precipitating minerals at the time it confirmed that the sulphides were separated as an immiscible liquid at the temperature point where orthopyroxene and clinopyroxene were both being formed. This is in agreement with the textures found within the samples. It has been suggested that the evidence collected shows that the melt that has formed the Harcus intrusion has already undergone a period of sulphide saturation before being emplaced leading to the lower concentrations in the metals of interest. An emplacement model for both intrusions has been proposed and suggests that the Harcus intrusion is more evolved than the Caroline intrusion.

Implications for Exploration

With the data that has been collected and the interpretations that have been made it can be said that Caroline style intrusions show more potential for economic ore body development than that of the Harcus intrusion. This is due to only having been through

one episode of sulphide saturation in its evolution and as such still being highly enriched in nickel and copper.

ACKNOWLEDGMENTS

Thanks must be given to Pepininni Minerals who provided the funding for this research, specifically Todd Williams and Angus Todd for their insights and guidance in the course of this research. John Foden and Nigel Cook are acknowledged for their work reviewing the manuscript in its many iterations. Angus Netting and Benjamin Wade are acknowledged for their support in the work carried out at Adelaide Microscopy, John Stanley and David Bruce for their support in the laboratory and analysis work carried out in the Mawson Laboratories, Christine Wawryk for her valuable conversations and help with regards to geochemical interpretation. Morgan Blades is thanked for her discussions on the implications of the isotope work that was undertaken and for her reviews of the manuscript. Katie Howard and Pam Carrol are thanked for their ongoing support throughout the course of the program. Ann Montgomery is thanked for her time in drafting the final manuscript.

REFERENCES

AITKEN A. R. & BETTS P. G. 2008. High-resolution aeromagnetic data over central Australia assist Grenville-era (1300–1100 Ma) Rodinia reconstructions. *Geophysical Research Letters* **35**, L01306.

AITKEN A. R. & BETTS P. G. 2009a. Multi-scale integrated structural and aeromagnetic analysis to guide tectonic models: An example from the eastern Musgrave Province, Central Australia. *Tectonophysics* **476**, 418-435.

AITKEN A. R. A. & BETTS P. G. 2009b. Constraints on the Proterozoic supercontinent cycle from the structural evolution of the south-central Musgrave Province, central Australia. *Precambrian Research* **168**, 284-300.

BAKER P. & WAUGH R. 2005. The role of surface geochemistry in the discovery of the Babel and Nebo magmatic nickel–copper–PGE deposits. *Geochemistry: Exploration, environment, analysis* **5**, 195-200.

CAWOOD P. A. & KORSCH R. 2008. Assembling Australia: Proterozoic building of a continent. *Precambrian Research* **166**, 1-35.

DEER W. A., HOWIE R. A. & ZUSSMAN J. 1966. An introduction to the rock-forming minerals.

EVINS P. M., SMITHIES R. H., HOWARD H. M., KIRKLAND C. L., WINGATE M. T. & BODORKOS S. 2010. Devil in the detail; The 1150–1000Ma magmatic and structural evolution of the Ngaanyatjarra Rift, west Musgrave Province, Central Australia. *Precambrian Research* **183**, 572-588.

FIORENTINI M. L., BEKKER A., ROUXEL O., WING B. A., MAIER W. & RUMBLE D. 2012. Multiple sulfur and iron isotope composition of magmatic Ni-Cu-(PGE) sulfide mineralization from eastern Botswana. *Economic Geology* **107**, 105-116.

FLEET M. E. 2006. Phase equilibria at high temperatures. *Reviews in Mineralogy and Geochemistry* **61**, 365-419.

GHIORSO M. S. & SACK R. O. 1995. Chemical mass transfer in magmatic processes IV. A revised and internally consistent thermodynamic model for the interpolation and extrapolation of liquid-solid equilibria in magmatic systems at elevated temperatures and pressures. *Contributions to Mineralogy and Petrology* **119**, 197-212.

GODEL B., SEAT Z., MAIER W. D. & BARNES S.-J. 2011. The Nebo-Babel Ni-Cu-PGE sulfide deposit (West Musgrave Block, Australia): Pt. 2. Constraints on parental magma and processes, with implications for mineral exploration. *Economic Geology* **106**, 557-584.

GUO J., GRIFFIN W. L. & O'REILLY S. Y. 1999. Geochemistry and origin of sulphide minerals in mantle xenoliths: Qilin, Southeastern China. *Journal of Petrology* **40**, 1125-1149.

JAYASURIYA K. D., O'NEILL H. S. C., BERRY A. J. & CAMPBELL S. J. 2004. A Mössbauer study of the oxidation state of Fe in silicate melts. *American Mineralogist* **89**, 1597-1609.

JUGO P. J. 2010. *Exponential Increase of Sulfur Content at Sulfide Saturation with Increasing Oxygen Fugacity: Implications for Cu-Ni-PGE Mineralization*. *11th International Platinum Symposium*.

KING A. 2007. Review of Geophysical Technology for Ni-Cu-PGE deposits. *Fourth Annual CIM Geological Society Conference. Sudbury*.

LI C., RIPLEY E. M. & NALDRETT A. J. 2003. Compositional variations of olivine and sulfur isotopes in the Noril'sk and Talnakh intrusions, Siberia: implications for ore-forming processes in dynamic magma conduits. *Economic Geology* **98**, 69-86.

LIGHTFOOT P. 2007. Advances in Ni-Cu-PGE Sulphide Deposit Models and Implications for Exploration Technologies. *Fourth Annual CIM Geological Society Conference. Sudbury*.

LIU Y., SAMAHA N.-T. & BAKER D. R. 2007. Sulfur concentration at sulfide saturation (SCSS) in magmatic silicate melts. *Geochimica et Cosmochimica Acta* **71**, 1783-1799.

LORAND J.-P. & GRÉGOIRE M. 2006. Petrogenesis of base metal sulphide assemblages of some peridotites from the Kaapvaal craton (South Africa). *Contributions to Mineralogy and Petrology* **151**, 521-538.

MAIER W. D. & GROVES D. I. 2011. Temporal and spatial controls on the formation of magmatic PGE and Ni–Cu deposits

Mineralium Deposita **46**, 841-857.

MAIER W. D., LI C. & DE WAAL S. A. 2001. WHY ARE THERE NO MAJOR Ni–Cu SULFIDE DEPOSITS IN LARGE LAYERED MAFIC-ULTRAMAFIC INTRUSIONS? *The Canadian Mineralogist* **39**, 547-556.

MAMUSE A., BERESFORD S., PORWAL A. & KREUZER O. 2010. Assessment of undiscovered nickel sulphide resources, Kalgoorlie Terrane, Western Australia: Part 1. Deposit and endowment density models. *Ore Geology Reviews* **37**, 141-157.

MCDONOUGH W., SUN S.-S., RINGWOOD A., JAGOUTZ E. & HOFMANN A. 1992. Potassium, rubidium, and cesium in the Earth and Moon and the evolution of the mantle of the Earth. *Geochimica et Cosmochimica Acta* **56**, 1001-1012.

MCDONOUGH W. F. & SUN S.-S. 1995. The composition of the Earth. *Chemical Geology* **120**, 223-253.

NALDRETT A. 1997. Key factors in the genesis of Noril'sk, Sudbury, Jinchuan, Voisey's Bay and other world-class Ni-Cu-PGE deposits: Implications for exploration. *Australian Journal of Earth Sciences* **44**, 283-315.

NALDRETT A. 1999. World-class Ni-Cu-PGE deposits: key factors in their genesis. *Mineralium Deposita* **34**, 227-240.

NALDRETT A. J. 2004. *Magmatic sulfide deposits: geology, geochemistry and exploration*. Berlin: Springer-Verlag.

NIMIS P. & TAYLOR W. R. 2000. Single clinopyroxene thermobarometry for garnet peridotites. Part I. Calibration and testing of a Cr-in-Cpx barometer and an enstatite-in-Cpx thermometer. *Contributions to Mineralogy and Petrology* **139**, 541-554.

PIRAJNO F. & HOATSON D. M. 2012. A review of Australia's Large Igneous Provinces and associated mineral systems: Implications for mantle dynamics through geological time. *Ore Geology Reviews* **48**, 2-54.

PUTIRKA K. D. 2008. Thermometers and barometers for volcanic systems. *Reviews in Mineralogy and Geochemistry* **69**, 61-120.

RIPLEY E. M. & LI C. 2013. Sulfide Saturation in Mafic Magmas: Is External Sulfur Required for Magmatic Ni-Cu-(PGE) Ore Genesis? *Economic Geology* **108**, 45-58.

RUTHERFORD L. 2010. Third Annual Technical Report for the Period Ending 23rd September 2010, EL3931 'Woodroffe', Musgrave Province, South Australia. *Pepinnini Minerals Limited* **SA Ex3931.03**.

RUTHERFORD L. 2011. Third Annual Technical Report for the Period Ending 25th Februaru 2011, EL4048 'Mt Caroline', Musgrave Province, South Australia. *Pepinnini Minerals Limited* **SA Ex4048.03**.

RUTHERFORD L. & CLIFFORD P. 2008. Third Annual Technical Report for the Period Ending 26th June 2008, EL3368 'Mt Harcus', Musgrave Province, South Australia. *Pepinnini Minerals Limited* **SA Ex3368.03**.

SEAT Z., BERESFORD S. W., GRGURIC B. A., GEE M. M. & GRASSINEAU N. V. 2009. Reevaluation of the role of external sulfur addition in the genesis of Ni-Cu-PGE deposits: Evidence from the Nebo-Babel Ni-Cu-PGE deposit, West Musgrave, Western Australia. *Economic Geology* **104**, 521-538.

SEAT Z., BERESFORD S. W., GRGURIC B. A., WAUGH R. S., HRONSKY J. M., GEE M. A. M., GROVES D. I. & MATHISON C. I. 2007. Architecture and emplacement of the Nebo–Babel gabbronorite-hosted magmatic Ni–Cu–PGE sulphide deposit, West Musgrave, Western Australia. *Mineralium Deposita* **42**, 551-581.

SEAT Z., GEE M. M., GRGURIC B. A., BERESFORD S. W. & GRASSINEAU N. V. 2011. The Nebo-Babel Ni-Cu-PGE sulfide deposit (West Musgrave, Australia): Pt. 1. U/Pb zircon ages, whole-rock and mineral chemistry, and O-Sr-Nd isotope compositions of the intrusion, with constraints on petrogenesis. *Economic Geology* **106**, 527-556.

TODD A. 2013. *Maps of tenements, magnetic and gravity*. Richardson C.

WADE B. P., KELSEY D. E., HAND M. & BAROVICH K. M. 2008. The Musgrave Province: stitching north, west and south Australia. *Precambrian Research* **166**, 370-386.

WINGATE M. T. D., PIRAJNO F. & MORRIS P. A. 2004. Warakurna large igneous province: A new Mesoproterozoic large igneous province in west-central Australia. *Geology* **32**, 105-108.

WOODHOUSE A. & GUM J. 2005. Musgrave Province - geological mapping update. *MESA* **38**, 35-38.